# Controls on nitrite oxidation in the upper Southern Ocean: insights from winter kinetics experiments in the Indian sector

Mhlangabezi Mdutyana[1,2*], Tanya Marshall[1], Xin Sun[3,4], Jessica M. Burger[1], Sandy J. Thomalla[2,5], Bess B. Ward[3] and Sarah E. Fawcett[1,5]

[1]Department of Oceanography, University of Cape Town, Rondebosch, South Africa
[2]Southern Ocean Carbon and Climate Observatory (SOCCO), CSIR, Rosebank, South Africa
[3]Department of Geosciences, Princeton University, Princeton, New Jersey, USA
[4]Department of Ecology and Evolutionary Biology, Yale University, New Haven, Connecticut, USA
[5]Marine and Antarctic Research centre on Innovation and Sustainability (MARIS), University of Cape Town, Rondebosch, Cape Town, South Africa

[*]Corresponding author: M. Mdutyana, mdtmhl001@myuct.ac.za

## Abstract

Across the Southern Ocean in winter, nitrification is the dominant mixed-layer nitrogen cycle process, with some of the nitrate produced therefrom persisting to fuel productivity during the subsequent growing season. Because this nitrate constitutes a regenerated rather than a new nutrient source to phytoplankton, it will not support net removal of atmospheric $CO_2$. To better understand the controls on Southern Ocean nitrification, we conducted nitrite oxidation kinetics experiments in surface waters across the western Indian sector in winter. While all experiments (seven in total) yielded a Michaelis-Menten relationship with substrate concentration, the nitrite oxidation rates only increased substantially once the nitrite concentration exceeded 115±2.3 to 245±18 nM, suggesting that nitrite oxidizing bacteria (NOB) require a minimum (i.e., "threshold") nitrite concentration to produce nitrate. The half-saturation constant for nitrite oxidation ranged from 134±8 to 403±24 nM, indicating a relatively high affinity of Southern Ocean NOB for nitrite, in contrast to results from culture experiments. Despite the high affinity of NOB for nitrite, its concentration rarely declines below 150 nM in the Southern Ocean's mixed layer, regardless of season. In the upper mixed layer, we measured ammonium oxidation rates that were two- to seven-fold higher than the coincident rates of nitrite oxidation, indicating that nitrite oxidation is the rate-limiting step for nitrification in the winter Southern Ocean. The decoupling of ammonium and nitrite oxidation, combined with a possible nitrite concentration threshold for NOB, may explain the non-zero nitrite that persists throughout the Southern Ocean's mixed layer year-round. Additionally, nitrite oxidation may be limited by dissolved iron, the availability of which is low across the upper Southern Ocean. Our findings have implications for understanding the controls on nitrification and ammonium and nitrite distributions, both in the Southern Ocean and elsewhere.

## 1. Introduction

The cycling of nitrogen (N) in the upper ocean is central to the role that phytoplankton and bacteria play in atmospheric carbon dioxide ($CO_2$) consumption and production. Annually, the Southern Ocean accounts for ~35% of total oceanic $CO_2$ removal (DeVries et al., 2017; Gruber et al., 2019; Watson et al., 2020) and absorbs ~40% of anthropogenic $CO_2$ (Khatiwala et al., 2009; Hauck et al., 2015; Gruber et al., 2019; Watson et al., 2020). The contribution of biology to $CO_2$ drawdown can be evaluated using the new production paradigm, among other approaches. This framework defines phytoplankton growth on nitrate ($NO_3^-$) supplied from below the euphotic zone as "new production" and phytoplankton growth on ammonium ($NH_4^+$) recycled within the euphotic zone as "regenerated production" (Dugdale and Goering 1967). Over appropriate timescales, new production is equivalent to "export production", the latter referring to the organic matter produced by phytoplankton that escapes recycling in surface waters and sinks into the ocean interior, thereby sequestering atmospheric $CO_2$ at depth (Dugdale and Goering, 1967; Eppley and Peterson ,1979; Volk and Hoffert, 1985; Raven and Falkowski, 1999). The occurrence of nitrification in the euphotic zone, which produces regenerated $NO_3^-$, complicates applications of the new production paradigm since phytoplankton growth fuelled by this $NO_3^-$ will drive no net removal of $CO_2$ (Yool et al., 2007).

In the Southern Ocean, nitrification appears to be largely confined to the dark waters below the euphotic zone during the summertime period of maximum $NO_3^-$ consumption by phytoplankton (DiFiore et al., 2009; Mdutyana et al., 2020). By contrast, the Southern Ocean winter is characterized by elevated mixed-layer nitrification rates, coincident with low rates of $NO_3^-$ uptake (Smart et al., 2015; Mdutyana et al., 2020). Some of the $NO_3^-$ regenerated in the winter mixed layer will be supplied to phytoplankton during the proceeding spring and summer growing season, with negative implications for $CO_2$ removal on an annual basis. That said, there is evidence that ammonia oxidizing archaea, the organisms that are dominantly responsible for $NH_4^+$ oxidation (the first step in the nitrification pathway) (Beman et al., 2008; Newell et al., 2011; Peng et al., 2016) have a high iron requirement (Shafiee et al., 2019), such that $NH_4^+$ oxidation may at times experience iron limitation ( Mdutyana et al. 2022). If this limitation is verified and proves widespread in the environment, one implication is that the iron-deplete conditions of the surface Southern Ocean may restrict mixed-layer nitrification and by extension, decrease the extent to which phytoplankton growth is fueled by regenerated nitrate.

Nitrification is a chemoautotrophic process involving two pathways usually facilitated by different groups of microorganisms. The first step is $NH_4^+$ oxidation, which involves the oxidation of $NH_4^+$ via hydroxylamine and nitric oxide to $NO_2^-$ (Walker et al. 2010; Vajrala et al. 2013; Kozlowski et al. 2016; Caranto and Lancaster 2017) by ammonia oxidizing archaea and bacteria (AOA and AOB, respectively; collectively, ammonia oxidizing organisms, AOO). The second step is the oxidation of $NO_2^-$ to $NO_3^-$ by

nitrite oxidizing bacteria (NOB), a polyphyletic group of microbes that is not well-understood in the ocean (Watson et al., 1986; Beman et al., 2013; Daims et al., 2016; Pachiadaki et al., 2017; Sun et al., 2021). In general, $NO_2^-$ oxidation rate data are limited, with few measurements available for the Southern Ocean (Bianchi et al. 1997; Mdutyana et al. 2020; Olson 1981a). Such measurements are critical, however, if we are to better understand the controls on nitrification in the Southern Ocean mixed layer and the connection between $NO_3^-$ production by NOB and its subsequent removal by phytoplankton.

One approach for investigating the controls on $NO_2^-$ oxidation is through experiments designed to yield a hyperbolic Michaelis-Menten relationship between $NO_2^-$ oxidation rate and $NO_2^-$ concentration. Useful kinetic parameters can be derived from this relationship, such as the maximum oxidation rate ($V_{max}$) and the half-saturation constant ($K_m$), with the latter indicating the $NO_2^-$ concentration at which the oxidation rate equals $V_{max}/2$. Estimates of $K_m$ provide information regarding the efficiency of NOB in acquiring substrate $NO_2^-$, with a lower $K_m$ indicating a higher affinity for $NO_2^-$, while $V_{max}$ denotes the maximum rate of $NO_2^-$ oxidation that can be achieved under a given set of conditions by a particular NOB community. In the ocean, direct measurements of $NO_2^-$ oxidation kinetic parameters are extremely limited (Olson, 1981; Sun et al., 2017, 2021; Zhang et al., 2020), with no estimates available for the Southern Ocean. $K_m$ values derived from culture studies of NOB range from 9-544 μM (Nowka et al., 2015; Ushiki et al., 2017), orders of magnitude higher than the existing estimates for natural assemblages of NOB in coastal waters and oxygen deficient zones (ranging from 0.07-0.51 μM; Olson, 1981; Sun et al., 2017; Zhang et al., 2020). This discrepancy emphasizes the gaps in our understanding of $NO_2^-$ oxidation and the organisms that catalyse it.

Generally, $NO_2^-$ concentrations in the low-latitude oxygenated ocean reach a maximum near the base of the euphotic zone (i.e., the primary nitrite maximum; PNM), with much lower concentrations above and below this depth (Lomas and Lipschultz 2006). By contrast, at higher latitudes including in the Southern Ocean, the $NO_2^-$ concentrations are elevated (100-400 nM) and fairly invariant throughout the mixed layer in all seasons (Zakem et al. 2018; Fripiat et al. 2019; Mdutyana et al. 2020). A possible explanation for this $NO_2^-$ accumulation is a decoupling of the $NH_4^+$ and $NO_2^-$ oxidation rates, with $NO_2^-$ oxidation being the rate-limiting step in the nitrification pathway, contrary to expectations for oxygenated marine waters (Kendall, 1998; Walker et al., 2010; Vajrala et al., 2013). However, this idea has yet to be examined using observations.

To better understand the controls on $NO_2^-$ oxidation (and thus, nitrification) in the Southern Ocean, we conducted a series of $NO_2^-$ oxidation kinetics experiments in wintertime surface waters across the western Indian sector. At every station (seven in total) along a transect between the Subtropical and Marginal Ice Zones, $NO_2^-$ oxidation rates increased with increasing $NO_2^-$ concentrations, as per the

expected Michaelis-Menten relationship. The derived $K_m$ values were low and increased with increasing ambient $NO_2^-$. Additionally, there appeared to be a minimum $NO_2^-$ concentration that was required before the $NO_2^-$ oxidation rates increased significantly, implying a "threshold" $NO_2^-$ requirement for $NO_2^-$ oxidation in the Southern Ocean. Finally, coincident measurements of euphotic zone $NH_4^+$ and $NO_2^-$ oxidation rates suggest that $NO_2^-$ oxidation is rate-limiting for nitrification across the Southern Ocean in winter.

## 2. Materials and Methods

### 2.1. Sampling site and experimental design

A winter cruise was undertaken onboard the R/V *SA Agulhas II* in July 2017 between Cape Town, South Africa, and the Marginal Ice Zone (MIZ; encountered at 61.7°S; de Jong et al., 2018), returning to South Africa along the meridional WOCE I06 transect (30ºE) (Figure 1). Sampling was conducted on two legs – between 37°S and 62°S on the southward leg (Leg 1) and between 59°S and 41°S on the northward return leg along the WOCE I06 line (Leg 2). During Leg 1, only surface samples were collected while on Leg 2, the deployment of conductivity-temperature-depth (CTD) hydrocasts allowed for depth-profile sampling.

*2.1.1 Hydrography and nutrient collections*: The positions of the major hydrographic fronts (the Subtropical Front, STF; Subantarctic Front, SAF; Polar Front, PF; and Southern Antarctic Circumpolar Current Front, SACCF; Figure 1) were determined from temperature and salinity measured by the ship's hull-mounted thermosalinograph (~7 m), augmented by temperature, salinity, and oxygen concentrations measured on Leg 2 by the CTD sensors (Orsi et al., 1995; Belkin and Gordon, 1996; Pollard et al., 2002; Read et al., 2002). For the hydrocast stations, the mixed layer depth was determined for each CTD (up)cast as the depth between 10 m and 400 m of maximum Brunt Väisälä frequency squared (i.e., $N^2$) (Schofield et al., 2015; Carvalho et al., 2017). Surface photosynthetically active radiation (PAR) was not measured continuously during the cruise; we thus use latitude as a qualitative proxy for light availability during Leg 1.

*2.1.2 Nutrient samples*: Seawater samples were collected every four hours from the ship's underway system (~7 m intake) on Leg 1 for the determination of $NO_2^-$ concentrations (Figure 1a). During Leg 2, samples were collected from Niskin bottles fired remotely between the surface and 500 m at eight hydrocast stations for the analysis of $NO_2^-$, $NO_3^-$, and $NH_4^+$ concentrations (see Figure 1b and c for station locations and sampling depths). For $NO_2^-$ and $NO_3^-$, unfiltered seawater was collected in duplicate 50 mL polypropylene centrifuge tubes that were analysed shipboard within 24 hours of collection ($NO_2^-$) or stored frozen at -20°C until analysis ($NO_3^-$). Seawater samples for $NH_4^+$ were

collected unfiltered in duplicate high-density polyethylene (HDPE) bottles that had been "aged" with orthophthaldialdehyde (OPA) working reagent, and analysed shipboard within 24 hours of collection.

*2.1.3 $NO_2^-$ oxidation kinetics experiments*: On Leg 1, seawater samples were collected from the surface via the ship's underway system at seven stations spanning the different zones of the Southern Ocean (the Subtropical Zone (STZ) to the north of the STF, at the STF, the Subantarctic Zone (SAZ) between the STF and SAF, the Polar Frontal Zone (PFZ) between the SAF and PF, the Open Antarctic Zone (OAZ) between the PF and SACCF, and the Marginal Ice Zone (MIZ) south of the SACCF; St 01 to St 07 in Figure 1a). At each station, 25 L of seawater were collected in a single carboy that was gently shaken to homogenize the contents before the seawater was filtered through a 200 µm nylon mesh to remove zooplankton grazers and then dispensed into 250 mL acid-washed opaque HDPE bottles. All the bottles were rinsed three times with sample water prior to filling. Eight sets of duplicate 250 mL bottles were amended with $Na^{15}NO_2$ to yield $^{15}NO_2^-$ concentrations ranging from 10 nM to 1500 nM.

*2.1.4 Depth distribution of $NO_2^-$ oxidation*: On Leg 2, seawater was collected at four stations (one each in the Polar Antarctic Zone (PAZ; just north of the edge of the MIZ), OAZ, PFZ, and SAZ; St 08 to St 11 in Figure 1a-c) using a CTD-rosette equipped with 24 12-L Niskin bottles. Seawater from six depths (10 m, 25 m, 50 m, 75 m, 200 m, and 500 m) was pre-filtered (200 µm nylon mesh) and transferred into rinsed 250 mL acid-washed opaque HDPE bottles. Duplicate bottles from each depth were amended with $Na^{15}NO_2$ to yield a final $^{15}NO_2^-$ concentration of 200 nM. From all incubation bottles (for kinetics and depth-profile experiments), initial ($T_0$) subsamples were collected in 50 mL centrifuge tubes immediately after the addition of $^{15}NO_2^-$. The opaque HDPE bottles from the upper 75 m were then incubated in custom-built on-deck incubators supplied with running surface seawater, while those from 200 m and 500 m were incubated in a ~2ºC cold room. The incubations lasted 23-30 hours and were terminated via the collection of final ($T_f$) subsamples (50 mL). Subsamples were filtered (0.2 µm) and stored frozen at -20°C until analysis.

*2.1.5 Depth distribution of $NO_3^-$ uptake*: To assess the extent to which mixed-layer $NO_2^-$ oxidation supports wintertime $NO_3^-$ uptake by phytoplankton, we also conducted $NO_3^-$ uptake experiments over the upper 75 m (the approximate depth of the euphotic zone) at St 08 to St 11 on Leg 2. Seawater was collected from four depths – 10 m, 25 m, 50 m, and 75 m – in duplicate 2 L clear polycarbonate bottles following filtration (200 µm nylon mesh) to remove large zooplankton grazers. $Na^{15}NO_3$ was added to each bottle to yield a final $^{15}NO_3^-$ concentration of 3 µM, and the bottles were then transferred to custom-built deck-board incubators equipped with neutral density screens that allowed for the penetration of 55%, 30%, 10%, and 1% of surface PAR. The bottles were kept at near *in situ* temperature via a supply of continuously-running seawater from the underway system. Samples were incubated for 3-6 hours, and incubations were terminated by filtering the bottle contents through pre-combusted (450°C for 8

hours) 0.3 µm glass fibre filters (GF-75; Sterlitech) that were subsequently enclosed in foil envelops (pre-combusted at 500°C for 5 hours) and stored at -80°C until analysis.

2.2. Laboratory analyses

*2.2.1 Nutrient concentrations*: Samples were analysed shipboard for $NO_2^-$ concentrations using the colorimetric method of Grasshoff et al., (1983) and a Thermo Scientific Genesys 30 Visible spectrophotometer (detection limit of 20 nM, precision of ±20 nM). $NO_3^-$+$NO_2^-$ concentrations were measured ashore using a Lachat Quick-Chem flow injection autoanalyzer (Egan, 2008) in a configuration with a detection limit of 0.2 µM and precision of ±0.3 µM. The concentration of $NO_3^-$ was determined by subtracting $NO_2^-$ from $NO_3^-$+$NO_2^-$. Aliquots of a certified reference material (JAMSTEC) were included in each $NO_2^-$ and $NO_3^-$+$NO_2^-$ run to ensure measurement accuracy. The $NH_4^+$ concentrations were also determined shipboard using the fluorometric method of Holmes et al. (1999); the methodological details and $NH_4^+$ data are discussed at length in (Mdutyana 2021) and (Smith et al., (2022).

*2.2.2 $NO_2^-$ oxidation rates:* Using the denitrifier-isotope ratio mass spectrometer (IRMS) method (Sigman et al., 2001; Weigand et al., 2016), we measured the $\delta^{15}N$ of $NO_3^-$ ($\delta^{15}N\text{-}NO_3^-$) produced from $^{15}NO_2^-$ oxidation for both the kinetics and depth-profile experiments ($\delta^{15}N$, in ‰ vs. air, = $(^{15}N/^{14}N_{sample}/^{15}N/^{14}N_{air} - 1) \times 1000$). Samples were measured using a Delta V Plus IRMS with a custom-built purge-and-trap front end ( Weigand et al., 2016) in a configuration with a detection limit of 0.2 nmol of N and a $\delta^{15}N$ precision of 0.2‰. Prior to isotope analysis, samples were treated with sulfamic acid (15 mM) to remove $^{15}NO_2^-$ remaining at the end of the experiments, after which sample pH was adjusted to ~7-8 via the addition of 2 M NaOH. To account for inefficiencies in $^{15}NO_2^-$ removal, both the $T_f$ and $T_0$ samples were treated with sulfamic acid prior to analysis of $\delta^{15}N\text{-}NO_3^-$ (more accurately, $\delta^{15}N\text{-}NO_3^-$+$NO_2^-$), with the difference between them taken as the $^{15}NO_3^-$ enrichment due to $^{15}NO_2^-$ oxidation (Peng et al., 2015). International reference materials (IAEA-N3, USGS 34, USGS 32) were used to calibrate the measured $\delta^{15}N\text{-}NO_3^-$.

The rate of $NO_2^-$ oxidation ($NO_2^-{}_{ox}$; nM $d^{-1}$) was calculated following Peng et al., (2015) as:

$$NO_2^-{}_{ox} = \frac{\Delta[^{15}NO_3^-]}{f_{NO_2^-}^{15} \times T} \quad (1)$$

Where $\Delta[^{15}NO_3^-]$ is the change in the concentration of $^{15}NO_3^-$ between the start and end of the incubation due to $NO_2^-$ oxidation, calculated from the difference in the measured $\delta^{15}N\text{-}NO_3^-$ between the $T_f$ and $T_0$ samples, $f_{NO_2^-}^{15}$ is the fraction of the $NO_2^-$ substrate pool labelled with $^{15}N$ at the start of the incubation,

calculated following the direct measurement of ambient $NO_2^-$ concentration, and T is the incubation length (days). Detection limits for $NO_2^-{}_{ox}$ rates ranged from 0.11 to 0.36 nM $d^{-1}$, calculated according to Santoro et al. (2013) and Mdutyana et al. (2020).

*2.2.3 Kinetic model:* Kinetic parameters are typically calculated using the Michaelis-Menten (MM) equation for enzyme kinetics (Monod, 1942):

$$V = \frac{V_{max} \times S}{K_m + S} \quad (2)$$

where V is the measured reaction rate, $V_{max}$ is the maximum reaction rate achievable under *in situ* conditions at saturating substrate (S) concentrations, and $K_m$ is the half-saturation constant, defined as the substrate concentration at which $V = V_{max}/2$.

The MM equation (equation 2) is a rectangular hyperbola, meaning that the asymptotes along the x- and y-axes are perpendicular. By definition, when S (the x-axis variable) is equal to zero, V (the y-axis variable) is also zero, forcing the model through the origin (0,0). In the case of $NO_2^-$ oxidation, the assumption that once $S > 0$, $V > 0$ is appropriate in waters where the ambient $NO_2^-$ concentration is near-zero or where $NO_2^-$ is non-zero but considerably lower than the $K_m$. In the Southern Ocean, mixed-layer $NO_2^-$ concentrations are typically ≥150 nM (Cavagna et al., 2015; Zakem et al., 2018; Fripiat et al., 2019; Mdutyana et al., 2020) and forcing the MM model through the origin results in a poor fit to the measurements (red line in Figure S1). This poor fit, in turn, leads to clearly inaccurate estimates of the kinetic parameters, particularly $K_m$ (Table S1).

While not typical for studies of $NO_2^-$ oxidation kinetics in the ocean, the standard form of non-linear regression models, including the MM equation, can be modified to better fit the observations (e.g., Birch, 1999; Tsoularis and Wallace, 2002; Archontoulis and Miguez, 2014). For application to our dataset, we modified equation 2 to allow $V = 0$ at $S > 0$ by subtracting a location parameter, C, from S (Figure 2) (Archontoulis and Miguez, 2014). In other words, we set the y-intercept (i.e., where $V = 0$) equal to C rather than to zero, which yields equation 3:

$$V = \frac{V_{max} \times (S-C)}{K_{m*} + (S-C)} \quad (3)$$

Using a non-linear, least-squares optimization method (Scipy lmfit package, Python 3.7.6), we solved equation 3 for $V_{max}$, $K_{m*}$, and C. The value of $K_{m*}$ derived in this way is relative to C, such that the substrate concentration at which $V = V_{max}/2$ (i.e., $K_m$) is actually equal to $K_{m*} + C$ (Supplemental Information). Mechanistically, C represents a "threshold" substrate concentration; when $S \leq C$, $V = 0$.

All derived kinetic parameters are reported as the best fit plus 95% confidence interval (i.e., mean ± 2σ; Table 1).

*2.2.4 Revising the depth distribution of $NO_2^-$ oxidation using $K_m$*: For the $NO_2^-$ oxidation experiments conducted at the Leg 2 hydrocast stations (i.e., depth-profile experiments; St 08 to St 11), the $Na^{15}NO_2$ was added to yield a final $^{15}NO_2^-$ concentration of 200 nM at all the sampled depths. However, at low ambient $NO_2^-$ concentrations (<1-2 μM), an amendment of this magnitude may stimulate $NO_2^-$ oxidation, leading to an overestimation of the *in-situ* rates. We thus revised our measured $NO_{2ox}^-$ rates using the derived $K_m$ values as per Rees et al. (1999), Diaz and Raimbault, (2000), and Horak et al. (2013):

$$\mathrm{corrNO}_{2\mathrm{ox}}^{-} = \frac{\mathrm{NO}_{2\mathrm{ox}}^{-}}{\frac{[\mathrm{NO}_2^-]_{\mathrm{total}}}{Km + [\mathrm{NO}_2^-]_{\mathrm{total}}} \times \frac{Km + [\mathrm{NO}_2^-]_{\mathrm{amb}}}{[\mathrm{NO}_2^-]_{\mathrm{amb}}}} \quad (4)$$

Here, $corrNO_{2ox}^-$ is the revised rate of $NO_{2ox}^-$, $NO_{2ox}^-$ is the measured $NO_2^-$ oxidation rate (equation 1), $[NO_2^-]_{amb}$ is the ambient $NO_2^-$ concentration measured at each depth, $[NO_2^-]_{total}$ refers to the concentration of $^{15}NO_2^-$ tracer plus $NO_{2amb}^-$, and $K_m$ is the derived half-saturation constant. We estimated a $K_m$ for each sample depth from the equation resulting from the linear regression of all derived $K_m$ values on $[NO_2^-]_{amb}$ (see section 4.2 below). We also computed $corrNO_{2ox}^-$ using the $K_m$ derived from the Leg 1 kinetics experiment located nearest each hydrocast station, which yielded very similar results. The values of $corrNO_{2ox}^-$ presented here were computed using the $K_m$ values derived from the linear regression equation. Rates of $NH_4^+$ oxidation measured coincident with $NO_{2ox}^-$ on Leg 2 (see Mdutyana et al., 2022 were similarly revised (to yield $corrNH_{4ox}^+$) using the $K_m$ values derived from kinetics experiments conducted during Leg 1 of the cruise – for St 08 and 09, $K_m$ =137 nM, for St 09, $K_m$ = 67 nM, and for St 11, $K_m$ = 28 nM.

*2.2.5 Isotopic dilution of $^{15}NO_2^-$ by co-occurring $NH_4^+$ oxidation:* The focus of this study is the second step in the nitrification pathway. However, not only will $NO_2^-$ have been consumed in our incubation bottles (i.e., oxidized to $NO_3^-$), but it will also have been produced by $NH_4^+$ oxidation, the first step in the nitrification pathway. For all of our $NO_2^-$ oxidation rate experiments (kinetics and depth-profile), we measured the coincident rates of $NH_4^+$ oxidation (Mdutyana et al., 2022), and these data can be used to account for any dilution of the $^{15}NO_2^-$ pool by $^{14}NO_2^-$ produced from $^{14}NH_4^+$ oxidation (following the approach of Glibert et al. (1982, 1985) and Mulholland and Bernhardt (2005 )). We found that isotopic dilution in the mixed layer was minor because the ambient $NO_2^-$ concentrations were reasonably high (mean of 157 ± 54 nM, range of 64 to 226 nM for all the depths at which experiments were conducted; Figure 1a-b) and the $NH_4^+$ oxidation rates were fairly low (mean of 13.4 ± 4.0 nM $d^{-1}$, range of 7.8 to 22.0 nM $d^{-1}$; see Figure 3f-j for the depth profile rates and Mdutyana et al., (2022) for the kinetics station

rates). Below the mixed layer where the ambient $NO_2^-$ concentrations were near-zero, so too were the $NH_4^+$ oxidation rates, which again resulted in minimal dilution of the $^{15}NO_2^-$ pool. Accounting for isotope dilution increased the $NO_2^-$ oxidation rates by 0 to 12% (mean of 3.9 ± 0.3% and median of 3.7 ± 0.3%), which is within the experimental error associated with the rate measurements; we thus consider the effect of isotope dilution to be negligible

*2.2.6 Nitrate uptake rates*: On shore, the GF-75 filters were oven-dried at 45°C for 24 hours, then pelletized into tin cups following the removal of unused peripheral filter. The concentration and isotopic composition of the particulate organic N (PON) captured on the filters was analyzed using a Delta V Plus IRMS coupled to a Flash 2000 elemental analyser, with a detection limit of 1 μg N and precision of ±0.005 At%. Blanks (combusted unused filters + tin capsules) and laboratory running standards calibrated to international reference materials were run after every five to ten samples. The absolute rates of $NO_3^-$ uptake ($\rho NO_3^-$; nM $d^{-1}$) were calculated after blank correction according to the equations of Dugdale and Wilkerson (1986) assuming a day-length of between 7 and 10 hours, depending on the station latitude. To compute the fraction of the mixed-layer $NO_3^-$ pool consumed by phytoplankton that derived from *in situ* nitrification, we trapezoidally-integrated $\rho NO_3^-$ and $corrNO_2^-{}_{ox}$ over the mixed layer following Mdutyana et al., (2020), and then divided the integrated values of $corrNO_2^-{}_{ox}$ by $\rho NO_3^-$.

## 3. Results

### 3.1 Hydrography and nutrient concentrations

The positions of the major hydrographic fronts during both legs of the cruise are shown in Figure 1a. At the hydrocast stations (Leg 2), the mixed layer depth (MLD) averaged 143 m in the OAZ, 146 m in the PFZ, 205 m in the SAZ, and 113 m in the STZ, which is within the reported climatological range for the western Indian sector of the Southern Ocean in winter (Sallée et al. 2010). Underway ambient $NO_2^-$ concentrations (Leg 1) ranged from 74 nM to 232 nM (transect average of 168 ± 48 nM, median of 177 nM) and generally increased with latitude, albeit with a high degree of variability (Figure 1a; Figure S2). The ambient $NO_2^-$ concentrations at the hydrocast stations were fairly constant throughout the mixed layer (ranging from 55 ± 35 nM to 159 ± 73 nM), decreasing rapidly to values below detection by 150-200 m (Figure 1b). Mixed-layer $NO_2^-$ showed no clear latitudinal trend, mainly because of the anomalously low concentrations measured at St 09 (54°S; mixed-layer average of 64 ± 30 nM, compared to 144 ± 56 for the seven other hydrocast stations). The $NO_3^-$ concentrations were also near-homogenous throughout the mixed layer, decreasing from an average of 28.4 ± 0.2 μM at the southernmost station (St 08; 59°S) to 3.7 ± 1.1 μM at the northernmost station (41°S), and increasing below the mixed layer as expected (Figure 1c).

### 3.2. $NO_2^-$ oxidation rates

*3.2.1 Kinetics experiments*: At all the kinetics stations (St 01 to St 07; Leg 1), an MM curve could be fit to the $NO_2^-$ oxidation rate *versus* substrate concentration measurements using equation 3 (Figure 2). The derived kinetic parameters varied across the transect (Table 1). The maximum $NO_2^-$ oxidation rate ($V_{max}$) increased southwards from 5.2 ± 0.1 nM $d^{-1}$ at the STF (St 02; Figure 2b) to 13 ± 0.4 nM $d^{-1}$ in the AZ (St 05; Figure 2e), before decreasing in the MIZ to 8.2 ± 0.1 nM $d^{-1}$ at St 06 (Figure 2f) and 6.6 ± 0.3 nM at St 07 (Figure 2g). The average $V_{max}$ for the transect was 9.0 ± 1.1 nM $d^{-1}$. The half-saturation constant ($K_m$) increased from 134 ± 8.0 nM at the STF (St 02) to 403 ± 24 nM in the MIZ (St 06), with a transect average of 277 ± 31 nM. The value of C showed a positive relationship with $[NO_2^-]_{amb}$ ($R^2$ = 0.59; $p$ = 0.045) and no strong relationship with latitude, and ranged from 115 ± 2.3 nM at the STF (St 02) to 245 ± 18 nM in the A Z (St 05), with a transect average of 181 ± 45 nM.

*3.2.2 Depth-profile experiments*: $NO_2^-$ oxidation rates at St 08 to St 11, calculated using equation 1, were low and largely invariant over the upper 75 m, ranging from 1.9 to 9.7 nM $d^{-1}$ (average of 4.9 ± 2.4 nM $d^{-1}$; filled symbols in Figure 3b-e). All stations showed a maximum $NO_2^-$ oxidation rate at 200 m (roughly coincident with or just below the MLD), ranging between 11 and 28 nM $d^{-1}$ (average of 18 ± 7.0 nM $d^{-1}$). The $NO_2^-$ oxidation rates showed a latitudinal gradient, with lower rates in the AZ (St 08 and 09) than in the PFZ (St 10) and SAZ (St 11).

Revising the $NO_2^-$ oxidation rates using equation 4 decreased their 0-75 m values by 13 to 26% (i.e., $corrNO_2^-{}_{ox}$ ranged from 1.6 to 8.5 nM $d^{-1}$ and averaged 4.0 ± 2.0 nM $d^{-1}$ over the upper 75 m; open symbols in Figure 3b-e). The largest decrease (of 39 to 68%) occurred at 200 m and 500 m, coinciding with the very low ambient $NO_2^-$ concentrations (Figure 3a) . Nonetheless, at all but St 08, the maximum $NO_2^-$ oxidation rate was still observed at 200 m, although its magnitude was lower. The coincidentally-measured and revised $NH_4^+$ oxidation rates ($corrNH_4^+{}_{ox}$) showed a similar pattern, with the largest decrease occurring at the depths with the lowest ambient $NH_4^+$ concentrations (Figure 3f-j) – over the upper 75 m, the rates decreased by 1 to 9% at St 08 to St 10 where the mixed-layer $NH_4^+$ concentrations averaged 263 ± 4.3 to 655 ± 15 nM, while at St 11 where the mixed-layer $NH_4^+$ concentration averaged 13 ± 1.6 nM, the rates decreased by 40 ± 23%. Similar to the $NO_2^-$ oxidation rates, the $NH_4^+$ oxidation rates decreased most at 200 m and 500 m, by between 33% and 70%. Hereafter, we use the revised $NO_2^-$ and $NH_4^+$ oxidation rates ($corrNO_2^-{}_{ox}$ and $corrNH_4^+{}_{ox}$, respectively) when referring to the depth distributions of these processes, including in Figures 5 and 6. We note, however, that the revised rates may still not be accurate since $K_m$ was not derived individually for each depth at each station (Horak et al., 2013). Nonetheless, because of the high concentration of the $^{15}N$-tracer amendments relative to all derived $K_m$ values, we are confident that the revised rates are more representative of *in situ* conditions than the rates computed using equation 1.

3.3 $NO_3^-$ uptake rates

The rates of $NO_3^-$ uptake ($\rho NO_3^-$) were low and relatively homogenous over the upper 75 m at each station (Figure S3a). Average euphotic zone $\rho NO_3^-$ increased northwards, from 2.9 ± 1.1 nM $d^{-1}$ at St 08 in the AZ to 12 ± 2.0 nM $d^{-1}$ at St 11 in the SAZ, with a transect average of 6.2 ± 3.4 nM $d^{-1}$. The euphotic zone PON concentrations also increased northwards, from 0.24 ± 0.02 μM at St 08 to 0.47 ± 0.08 μM at St 11 (Figure S3b). Integrated over the mixed layer, $corrNO_2^-{}_{ox}$ accounted for an average of 122% of $\rho NO_3^-$ (range of 63% at St 09 to 237% at St 08 in the AZ; Table S2), consistent with previous observations from the wintertime Southern Ocean (Mdutyana et al., 2020).

## 4. Discussion

Across all the major zones of the wintertime Southern Ocean, the addition of $NO_2^-$ to samples of surface seawater stimulated $NO_2^-$ oxidation following a Michaelis-Menten relationship, suggesting that substrate availability plays a dominant role in determining the rate of $NO_3^-$ production in the Southern Ocean's winter mixed layer. Curiously, however, we also observed an apparent minimum substrate requirement of $NO_2^-$ oxidation (i.e., a "threshold" $NO_2^-$ concentration, ranging from 115 to 245 nM), which contradicts expectations for a "classical" Michaelis-Menten relationship (i.e., V is expected to increase as soon as S > 0, assuming S is limiting to V; Monod, 1942). Below, we examine our findings in the context of existing estimates of $NO_2^-$ oxidation kinetic parameters and then evaluate the potential drivers of the trends that we observe. We also discuss possible reasons for the apparent requirement of Southern Ocean NOB for a threshold ambient $NO_2^-$ concentration and consider the implications thereof for the regional N cycle.

### 4.1 Southern Ocean $NO_2^-$ oxidation kinetic parameters in the context of existing estimates

Measurements of $NO_2^-$ oxidation rates are limited in the Southern Ocean, with only two studies that have directly measured this pathway in open-ocean waters (Bianchi et al. 1997; Mdutyana et al. 2020). For $NO_2^-$ oxidation kinetics, there are no data at all for the Southern Ocean. This scarcity of measurements is unsurprising given that *in situ* $NO_2^-$ oxidation kinetics studies are generally limited; indeed, to our knowledge, there are only two studies from the coastal ocean (Olson 1981a; Zhang et al. 2020) and two from the Eastern Tropical North Pacific oxygen deficient zone (ETNP ODZ; with these experiments conducted across a range of ambient oxygen concentrations; Sun et al., 2017, 2021). By contrast, there exist numerous estimates of $NO_2^-$ oxidation kinetic parameters determined using cultured marine NOB (e.g., Sorokin et al., 2012; Nowka et al., 2015; Jacob et al., 2017; Kits et al., 2017; Zhang et al., 2020). In general, culture experiments suggest far higher kinetic constants compared to the limited *in situ* observations from the ocean, particularly for $K_m$ (i.e., culture-based $K_m$ estimates of 9-544 μM; Blackburne et al., 2007; Nowka et al., 2015; Ushiki et al., 2017).

The high $K_m$ values derived for cultured NOB suggest that the affinity of these organisms for $NO_2^-$ is low. However, this is not what is observed in the environment, which indicates that the most abundant marine NOB are not represented in the culture collection. For the Southern Ocean, we report high substrate affinities of NOB, with $K_m$ values ranging from 134 to 403 nM, which is largely within the range documented for oxygenated coastal and open ocean waters (27-506 nM; Olson, 1981; Zhang et al., 2020) (Table 2). In the low- to zero-oxygen waters of the ETNP ODZ, similarly low $K_m$ values have been reported (254 ± 161 nM; Sun et al., 2017), although values >5 µM have also been observed (Sun et al., 2021), with these latter estimates associated with ambient $NO_2^-$ concentrations >1 µM. We explore the relationship between ambient $NO_2^-$ concentration and $K_m$ in detail in section 4.2 below. Our focus is on the $K_m$ values derived under conditions of low ambient $NO_2^-$ (i.e., <250 nM) given that (some of) the environmental factors affecting $NO_2^-$ oxidation at high ambient $NO_2^-$ concentrations appear to be unique. For example, oxygen has been shown to decrease the rate of $NO_2^-$ oxidation in the ODZs (Sun et al., 2017, 2021) where novel clades of NOB have been detected (Sun et al., 2021). Additionally, $NO_2^-$ concentrations in the oxygenated open ocean seldom exceed 250 nM (Zakem et al., 2018), in contrast to the ODZs (Bristow et al., 2016; Füssel et al., 2012).

Across our Southern Ocean transect, $V_{max}$ ranged from 5 to 14 nM $d^{-1}$, which is relatively low compared to estimates from other regions (Table 2), although such a comparison may not be particularly informative as our rates (and typically those of others) are not normalized for NOB abundance. Our $V_{max}$ estimates are also low compared to a previous study of mixed-layer nitrification in the winter Southern Ocean (Mdutyana et al., 2020). This difference may be partly due to the fact that the kinetics experiments were conducted using surface (~7 m) seawater (and thus, the surface NOB community that had been exposed to surface conditions, including elevated light), yet the highest rates of $NO_2^-$ oxidation typically occur near the base of the mixed layer, including in the Southern Ocean (Figure 3b-e; Sun et al., 2017; Peng et al., 2018; Mdutyana et al., 2020). The opposite pattern has also been observed, however(although not in the Southern Ocean), with deeper samples yielding a lower $V_{max}$ than samples collected in shallow waters (Sun et al., 2017; Zhang et al., 2020).

### 4.2 Environmental drivers of the $NO_2^-$ oxidation kinetic parameters

We report maximum $NO_2^-$ oxidation rates that generally increase towards the south and with decreasing SST (recognizing that these parameters co-vary), although St 01 in the STZ and St 06 and 07 in the MIZ deviate from this trend (Figure 4a and b; $R^2 = 0.019$; $p = 0.77$ and $R^2 = 0.12$; $p = 0.45$, respectively when all the stations are considered and $R^2 = 0.92$; $p = 0.041$ and $R^2 = 0.94$; $p = 0.029$, respectively, when St 01, 06, and 07 are excluded). It is possible that changes in the NOB community (composition and/or abundance) across the transect explains some of the observed variability. Nonetheless, taking latitude as a qualitative proxy for light, it is perhaps unsurprising that the maximum $NO_2^-$ oxidation

rates increase southwards given that NOB are known to be at least partially light inhibited (Peng et al., 2018; Ward, 2005; Olson, 1981b). This explanation does not hold for the stations in the MIZ, however, at which $V_{max}$ decreases sharply despite these waters receiving the least light (less than 5 hours of weak sunlight, versus ~7 hours at 55ºS to ~9 hours at 37ºS). The temperature at the MIZ stations was <0°C, which raises the possibility of a temperature effect on $V_{max}$. Indeed, we previously observed a strong decline in the $V_{max}$ associated with $NH_4^+$ oxidation at SSTs <0°C in the Southern Ocean, while at SSTs ranging from 0.6°C to 16°C, $V_{max}$ was near invariant (Mdutyana et al., 2022).

Marine nitrification has been reported to be largely unaffected by temperature variations (Bianchi et al., 1997; Horak et al., 2013; Baer et al., 2014), although $NH_4^+$ and $NO_2^-$ oxidation may respond differently to similar changes in temperature. For example, marine NOB incubated at temperatures ranging from 10°C to 35°C responded far more slowly to an increase in temperature than co-incubated AOA, resulting in an accumulation of $NO_2^-$ in the incubation bottles (Schaefer and Hollibaugh 2017). By contrast, we previously observed no robust relationship between temperature and the maximum $NH_4^+$ oxidation rate in the Southern Ocean (Mdutyana et al., 2022), a finding that is consistent with studies of $NH_4^+$ oxidation in the Arctic and temperate coastal ocean (Horak et al., 2013; Baer et al., 2014). Far less work has been done to assess the response of NOB to temperature changes. In the absence of experiments specifically designed to test the response of Southern Ocean NOB to temperature, it is difficult to disentangle the effect(s) on $NO_2^-$ oxidation of temperature *versus* light (and possibly other parameters that co-vary with latitude, such as $NO_2^-$ and/or micronutrient availability).

Plotting $V_{max}$ as a function of the ambient substrate concentration ($[NO_2^-]_{amb}$) reveals a strong positive relationship for all but the MIZ stations (Figure 4c; $R^2 = 0.73$; $p = 0.065$ if the MIZ stations are excluded). In particular, the STZ station (St 01), which appeared anomalous in the plots of $V_{max}$ versus latitude and SST, is consistent with the other non-MIZ stations when evaluated in $V_{max}$ versus $[NO_2^-]_{amb}$ space. The positive relationship of $V_{max}$ to $[NO_2^-]_{amb}$ could be taken as evidence that $NO_2^-$ availability strongly controls the maximum achievable rate of $NO_2^-$ oxidation. However, $V_{max}$ varies four-fold across the transect while $[NO_2^-]_{amb}$ only changes by a factor of two, and $[NO_2^-]_{amb}$ is also correlated with latitude ($R^2 = 0.51$, $p < 0.001$ for all surface $[NO_2^-]_{amb}$ data; Figure S2). Additionally, previous wintertime Southern Ocean $NO_2^-$ oxidation rates (albeit not $V_{max}$) showed no relationship with ambient $NO_2^-$ concentration (Bianchi et al. 1997; Mdutyana et al. 2020). The extent to which $V_{max}$ is directly controlled by $[NO_2^-]_{amb}$ is thus unclear, and it is likely that NOB community composition, light availability, and temperature also play a role, with SST perhaps becoming more important at very low temperatures (i.e., in the MIZ).

Our estimates of $K_m$ reveal that NOB in the wintertime Southern Ocean have a high affinity for $NO_2^-$ that appears to decrease (i.e., the $K_m$ rises) at higher latitudes (i.e., lower light) and lower temperatures,

with St 01 in the STZ again emerging as an exception (Figure 4d and e; $R^2 = 0.86$, $p = 0.008$ and $R^2 = 0.86$, $p = 0.008$, respectively). Plotting our $K_m$ values as a function of $[NO_2^-]_{amb}$ reveals a strong positive relationship (Figure 4f; $R^2 = 0.83$, $p = 0.004$; black data points), implying that $NO_2^-$ availability rather than temperature or light exerts the dominant control on $K_m$. This trend further suggests that NOB are well-adapted to the environment (or Southern Ocean region) in which they are found. Southern Ocean mixed-layer $NO_2^-$ concentrations are almost never <150 nM, regardless of the season (Fripiat et al. 2019; Mdutyana et al. 2020; Zakem et al. 2018), yet the relationship of $K_m$ to $[NO_2^-]_{amb}$ also holds at far lower $NO_2^-$ concentrations. The coloured data points in Figure 4f show $K_m$ versus $[NO_2^-]_{amb}$ for four additional regions where a Michaelis-Menten relationship of $NO_2^-$ oxidation rate to $NO_2^-$ concentration was observed and where $[NO_2^-]_{amb}$ was <250 nM (two coastal ocean sites, the South China Sea (SCS; Zhang et al., 2020) and Southern California Bight (SCB; Olson, 1981); one oligotrophic ocean site, the subtropical South Atlantic (SSA; Fawcett et al. unpubl.); and two stations from the ETNP ODZ, where oxygen concentrations ranged from 0 μM to 16.8 μM (Sun et al., 2017)). The robust positive relationship of $K_m$ to $[NO_2^-]_{amb}$ that emerges when these previous results are combined with our Southern Ocean data ($R^2 = 0.68$, $p < 0.001$) strongly implicates $[NO_2^-]_{amb}$ as the dominant control on the $K_m$ of $NO_2^-$ oxidation in the ocean, particularly at low $[NO_2^-]_{amb}$ (i.e., <250 nM).

The production of $NO_2^-$ from $NH_4^+$ oxidation has recently been hypothesized to be vulnerable to iron limitation (Mdutyana et al., 2022) since AOB rely on iron-rich *cytochrome c* proteins (Arp et al., 2002; Walker et al., 2010) and some AOA appear to have a low affinity for inorganic iron (Shafiee et al. 2019). NOB also contain iron-rich enzymes, such as nitrite oxidoreductase, which is responsible for converting $NO_2^-$ to $NO_3^-$ (Meincke et al., 1992; Spieck et al., 1998). While we have no iron data with which to compare our kinetic parameters, dissolved iron concentrations ([DFe]) were measured throughout the euphotic zone at the depth-profile stations (St 08 to St 11; Mdutyana et al., 2022). The revised $NO_2^-$ oxidation rates at these stations are weakly positively correlated with [DFe] ($R^2 = 0.35$, $p = 0.016$; Figure 5), indicating a potential role for iron in controlling $NO_2^-$ oxidation. Combined with the evidence that iron may also constrain marine $NH_4^+$ oxidation (Shafiee et al., 2019), this observation implies that mixed-layer nitrification in the Southern Ocean may be iron-limited. Since phytoplankton consumption of regenerated $NO_3^-$ yields no net removal of atmospheric $CO_2$ in a mass balance sense (Dugdale and Goering 1967; Yool et al., 2007), an iron-related control on mixed-layer nitrification would help to limit the extent to which this process can weaken the Southern Ocean's biological pump and would lead to enhanced competition between phytoplankton and nitrifiers for iron.

### 4.3 The persistence of elevated $NO_2^-$ concentrations throughout the Southern Ocean's mixed layer

While still limited, there is growing evidence that marine AOA have a very high affinity for $NH_4^+$ (more correctly, ammonia ($NH_3$), the substrate for $NH_4^+$ oxidation; Mdutyana et al., 2022; Martens-Habbena et al., 2009; Horak et al., 2013; Newell et al., 2013; Peng et al., 2016). Marine NOB also appear able to access low concentrations of substrate, based on the few *in situ* studies conducted to-date, including this one (Figure 4f; Olson, 1981; Sun et al., 2017; Zhang et al., 2020). This high substrate affinity is perhaps unsurprising given that $NO_2^-$ concentrations are generally near-zero throughout the oxygenated ocean, rising modestly to values typically <500 nM at the PNM in (sub)tropical waters (Lomas and Lipschultz 2006; Zakem et al. 2018) and <400 nM over the mixed layer in (sub)polar regions (Zakem et al., 2018). The average surface $NO_2^-$ concentration measured during Leg 1 of our cruise was 168 ± 48 nM (Figure 1a) and the average mixed-layer concentration for Leg 2 was 137 ± 57 nM (Figures 1b and 3a). Similar concentrations have been observed previously across the Southern Ocean, including in other seasons (Cavagna et al., 2015; Fripiat et al., 2019; Mdutyana et al., 2020). Thus, while $NO_2^-$ oxidation in Southern Ocean surface waters is characterized by a low $K_m$, the affinity of NOB for $NO_2^-$ is apparently not high enough to completely remove the available $NO_2^-$.

The persistence of elevated $NO_2^-$ concentrations in the mixed layer at high latitudes has previously been attributed to the inability of iron- and/or light-limited phytoplankton to fully consume $NO_2^-$ transported to the surface with $NO_3^-$ during deep mixing events (Zakem et al. 2018). However, subsurface $NO_2^-$ concentrations in the Southern Ocean are typically below detection (Figure 1b and 3a; Olsen et al., 2016), so it is unclear how deep mixing could supply measurable $NO_2^-$ to the euphotic zone. We thus discount subsurface mixing as a primary explanation for the elevated Southern Ocean mixed-layer $NO_2^-$ concentrations, as were observed during our study and in other seasons (e.g., Fripiat et al., 2019).

A second possible source of elevated mixed-layer $NO_2^-$ is efflux following partial $NO_3^-$ reduction to $NO_2^-$ by phytoplankton (Lomas and Lipschultz 2006), which has been extensively documented in laboratory and field studies (see Collos, 1998 for a review). The release of $NO_2^-$ by phytoplankton is hypothesized to result from light limitation of intracellular $NO_2^-$ reduction (Vaccaro and Ryther 1960; Kiefer, Olson, and Holm-Hansen 1976), short-term increases in irradiance to which phytoplankton cannot adapt (Lomas and Lipschultz 2006), iron limitation of $NO_3^-$ assimilation (Milligan and Harrison 2000), and/or release of phytoplankton from $NO_3^-$ limitation following a period of starvation (Sciandra and Amara 1994). While some of these mechanisms may be ongoing in the Southern Ocean, they all require the initial uptake of $NO_3^-$ by phytoplankton. This process occurs in the winter mixed layer at rates that are too low to support $NO_2^-$ efflux to the extent that it would allow $NO_2^-$ to accumulate to concentrations of 100-400 nM (Figure S3; Philibert et al., 2015; Mdutyana et al., 2020) while simultaneously being removed by $NO_2^-$ oxidation. Additionally, we observe a reasonable correlation

between the $NH_4^+$ oxidation rates and the ambient $NO_2^-$ concentration ($R^2 = 0.46$, $p < 0.001$; Figure S4), which implies that $NO_2^-$ derives mainly from $NH_4^+$ oxidation rather than phytoplankton efflux.

A third potential explanation for elevated mixed-layer $NO_2^-$ is a decoupling of $NH_4^+$ and $NO_2^-$ oxidation, which appears to be widespread in the environment (e.g., Ward and Zafiriou, 1988; Beman et al., 2013). In the oxygenated ocean, $NH_4^+$ oxidation has been considered the rate-limiting step in the nitrification pathway because $NO_2^-$ seldom accumulates in the mixed layer (Kendall 1998; Kowalchuk and Stephen 2001; Walker et al. 2010; Vajrala et al. 2013). However, rate measurements from numerous ocean regions show contrasting results, with $NO_2^-$ oxidation sometimes outpacing $NH_4^+$ oxidation (Peng et al. 2018; Dore and Karl 1996; Bristow et al. 2015; Horrigan et al. 1990) while in other cases, $NH_4^+$ oxidation is dominant (Ward and Kilpatrick 1991; Kalvelage et al. 2013; Clark et al. 2008). The limited data available from previous Southern Ocean investigations show no clear trend (Bianchi et al., 1997; Mdutyana et al., 2020). In the present study, mixed-layer $corrNO_2^-{}_{ox}$ rates are two- to seven-times lower than the coincidentally measured $corrNH_4^+{}_{ox}$ (Figures 3 and 6). Additionally, the maximum rates of $NO_2^-$ oxidation ($V_{max}$) that we measure in this study for the surface NOB community (~5 to 13 nM $d^{-1}$; Figure 2) are on average half those determined at the same stations for $NH_4^+$ oxidation (14 to 23 nM $d^{-1}$; Mdutyana et al., 2022). At the time of our sampling, therefore, $NO_2^-$ oxidation was rate-limiting for nitrification, which likely accounts for much of the $NO_2^-$ accumulated in the Southern Ocean's winter mixed layer .

If a decoupling of $NH_4^+$ and $NO_2^-$ oxidation is predominantly responsible for $NO_2^-$ accumulation, an obvious question is why these rates are not balanced. Environmental factors like temperature and light may play a role (Ward, 2008), as may iron limitation and the different ecophysiologies of $NH_4^+$ and $NO_2^-$ oxidizers. AOA have been shown to adapt more rapidly than NOB to a change in temperature (Schaefer and Hollibaugh, 2017); however, seasonal SST changes within the various zones of the Southern Ocean are fairly small and the aforementioned study showing the differential thermal response of AOA and NOB was conducted at higher temperatures than those experienced in much of the Southern Ocean. With regards to light, there is evidence from culture and field studies that NOB are more photosensitive than AOA and AOB (Bock, 1965; Olson, 1981b; Qin et al., 2014). Our data are consistent with this notion insofar as the $V_{max}$ associated with $NO_2^-$ oxidation in surface waters rises with increasing latitude (and thus decreasing light; Figure 4a) while the $V_{max}$ derived for $NH_4^+$ oxidation remains largely unchanged across >30 degrees of latitude (Mdutyana et al., 2022). However, the ambient $NO_2^-$ concentration in Southern Ocean surface waters rises near linearly with latitude (Figure S2a) while the $NH_4^+$ concentration resembles a step function, increasing from ~100 nM north of the SAF to ~700 nM south of the SAF, over a distance of roughly one degree of latitude (Figure S2b). The differing trends in $V_{max}$ may thus have more to do with substrate availability than photoinhibition.

584 Mixing, particularly deep winter overturning, might also contribute to a decoupling of $NH_4^+$ and $NO_2^-$
585 oxidation. In coastal waters, deep winter mixing has been shown to dilute the nitrifier community, with
586 AOO subsequently observed to recover more rapidly than NOB. This differential rate of recovery has
587 been hypothesized to result in a period of low rates of $NO_2^-$ oxidation during which the co-occurring
588 $NH_4^+$ oxidation rates remain elevated, ultimately causing $NO_2^-$ to accumulate in the surface layer (Haas
589 et al., 2021). While a similar effect may play a role in $NO_2^-$ accumulation in the open Southern Ocean,
590 it is unlikely that the entire $NO_2^-$ reservoir can be attributed to this process. The rates of $NH_4^+$ oxidation
591 are only slightly higher than the $NO_2^-$ oxidation rates in the winter mixed layer (Figure 3) and the mixed-
592 layer $NH_4^+$ concentrations are elevated (Figure 3f). These observations imply that $NH_4^+$ oxidizers are
593 limited by something other than $NH_4^+$ substrate, ). These observations them from catalysing higher rates
594 of $NO_2^-$ production (and thus $NO_2^-$ accumulation).
595
596 Nitrite oxidoreductase (NXR), the enzyme possessed by NOB that is responsible for aerobic $NO_2^-$
597 oxidation to $NO_3^-$, is an iron-sulfur molybdoprotein (Sundermeyer-Klinger et al. 1984; Meincke et al.
598 1992; Lücker et al. 2010). As such, $NO_2^-$ oxidation has a significant iron requirement (Saito et al., 2020;
599 Bayer et al., 2021), intimated by the relationship we observe between $corrNO_2^-{}_{ox}$ and DFe (Figure 5).
600 Additionally, $NO_2^-$ accumulation at the PNM in the California Current has been hypothesized to be
601 caused by iron limitation of NOB (Santoro et al. 2013). AOB also require iron, in particular for the
602 oxidation of hydroxylamine, which is catalyzed by the heme-rich hydroxylamine oxidoreductase
603 complex (Arp et al., 2002; Walker et al., 2010). By contrast, AOA, the dominant marine $NH_4^+$ oxidizers,
604 rely mainly on copper-containing proteins to mediate $NH_4^+$ oxidation (Amin et al., 2013; Walker et al.,
605 2010; Santoro et al., 2015). In the iron-limited Southern Ocean, it is thus possible that iron scarcity
606 more strongly limits $NO_2^-$ than $NH_4^+$ oxidation. However, recent culture and proteomic work suggests
607 that some AOA may actually have a high iron requirement (Alyson E. Santoro et al. 2015; Carini,
608 Dupont, and Santoro 2018; Qin et al. 2018; Shafiee et al. 2019), and we have previously hypothesized
609 an iron-related control on $NH_4^+$ oxidation in the Southern Ocean (Mdutyana et al., 2022). Deeper
610 investigation is thus required to characterize the role of iron in controlling the relative rates of $NH_4^+$ and
611 $NO_2^-$ oxidation, and the implications for the complete nitrification pathway.
612
613 A further consideration is differences in the ecology of AOA and NOB. Marine NOB are an order of
614 magnitude less abundant than AOA (e.g., Füssel et al., 2012; Beman et al., 2013b; Pachiadaki et al.,
615 2017; Damashek et al., 2019; Kitzinger et al., 2020) and roughly three-times larger (Watson and
616 Waterbury, 1971; Könneke et al., 2005; Martens-Habbena et al., 2009; Pachiadaki et al., 2017). While
617 marine NOB appear to have a high affinity for ambient $NO_2^-$, the *in situ* $K_m$ values derived to-date are
618 not as low as those reported for $NH_4^+$ oxidation (Horak et al., 2013; Peng et al., 2016; Xu et al., 2019;
619 Zhang et al., 2020; Mdutyana et al. 2022), which is perhaps to be expected given the larger size of
620 NOB versus AOA. Resource limitation theory posits that nitrifiers (NOB and AOA) require a

subsistence concentration of substrate (R*) to maintain their population, and that those with the lowest R* will outcompete all other organisms limited by the same resource, provided that their $V_{max}$ is higher than their loss rate due to grazing and/or viral lysis (Zakem et al., 2018). Because NOB are larger than AOA, they will have a higher R* even before grazing pressure is factored in. Their larger size also means that NOB are more likely to be grazed than AOA, which will further increase their R*, as will the fact that their maximum growth rates are low and thus vulnerable to being outpaced by their loss rate. Taken together, these factors will increase R*, potentially resulting in the accumulation of $NO_2^-$ in the water column, and may help to explain why the $K_m$ for $NO_2^-$ oxidation, in the Southern Ocean and elsewhere, is considerably higher than the $K_m$ derived for $NH_4^+$ oxidation. Additionally, the fact that NOB will be preferentially grazed over AOA may contribute to $NO_2^-$ oxidation being rate-limiting for nitrification.

That $NO_2^-$ oxidation was rate-limiting at the time of our sampling does not necessarily explain the accumulation of $NO_2^-$ in the Southern Ocean mixed layer year-round. Neither $NH_4^+$ nor $NO_2^-$ oxidation occur at elevated rates in summer or autumn (Bianchi et al., 1997; Mdutyana et al., 2020), yet the elevated $NO_2^-$ concentrations persist during these seasons (Cavagna et al., 2015; Fripiat et al., 2019; Mdutyana et al., 2020). To fit a Michaelis-Menten function to our experimental data required amending the classical equation (equation 2) to allow for a positive x-intercept (i.e., a non-zero S value at which V was still zero, the C parameter in equation 3) (Archontoulis and Miguez, 2014). Additionally, at most stations, the $NO_2^-$ oxidation rates did not increase substantially following the initial two or three substrate amendments (i.e., in Figure 2, the slope of the relationship between V and S is less steep for the initial two to three values of S than at higher S values). Practically, our findings suggest that Southern Ocean NOB require a minimum (i.e., "threshold") $NO_2^-$ concentration below which the $NO_2^-$ concentration becomes severely limiting. Coupled with weak $NO_2^-$ drawdown by iron- and/or light-limited phytoplankton during their incomplete consumption of the $NO_3^-$+$NO_2^-$ pool, a threshold substrate requirement of NOB can explain the year-round persistence of non-zero mixed-layer $NO_2^-$ since it implies that there is no mechanism by which $NO_2^-$ can be completely exhausted.

The existence of a $NO_2^-$ concentration threshold may indicate limitation of the membrane-bound NXR enzyme, either by $NO_2^-$ or by another essential nutrient. Recently, using NXR concentrations, estimates of NXR specific activity, and direct measurements of *in situ* $NO_2^-$ oxidation rates, Saito et al., (2020) deduced that *Nitrospina* NXR is undersaturated with $NO_2^-$ in the tropical Pacific, possibly due to iron limitation. The authors suggest that under iron-scarce conditions, it becomes increasingly difficult for NOB to synthesize NXR and thus to oxidize $NO_2^-$. A similar dynamic may be at play in the Southern Ocean, with limited synthesis of NXR at low iron concentrations resulting in a decrease in the efficiency of the $NO_2^-$ oxidation pathway that manifests most strongly when the ambient $NO_2^-$ concentration is also low. This inefficiency could be alleviated at higher $NO_2^-$ concentrations since NOB (even with a

paucity of NXR) are less likely to experience diffusion limitation with respect to $NO_2^-$ when there is more of this substrate available (Pasciak and Gavis 1974). Regardless of its mechanistic basis, limitation of NOB NXR would help to explain the perennially high concentrations of $NO_2^-$ in the Southern Ocean mixed layer. Moreover, environmental factors unique to the Southern Ocean, such as limited iron availability, may be instrumental in setting the $NO_2^-$ threshold and associated elevated mixed-layer $NO_2^-$ concentrations.

Our observations raise the question of why a similar $NO_2^-$ concentration threshold has not been reported for other ocean regions, particularly those characterized by similar conditions to the Southern Ocean. This may partly be due to the very limited number of $NO_2^-$ oxidation kinetics experiments that have been conducted in the open ocean and/or to the fact that a classic Michaelis-Menten function is usually imposed upon kinetics data, with V assumed to increase as soon as S > 0. Additionally, depending on the maximum substrate concentration added during kinetics experiments (i.e., the maximum concentration on the x-axis of the V versus S plot), it can be difficult to discern a possible threshold $NO_2^-$ concentration by simply examining the plots. Inspection of published Michaelis-Menten curves does reveal the possibility of a non-zero C value in some cases, including in the ETNP ODZ (Sun et al., 2021) and associated with the PNM in the South China Sea (Zhang et al., 2020). However, there are also published curves that clearly intercept the origin in V versus S space (Olson, 1981a; Sun et al., 2017), underscoring the need for further investigation of the conditions that lead to a threshold $NO_2^-$ concentration requirement of NOB.

## 5. Concluding remarks

In this study, we present the first $NO_2^-$ oxidation kinetic constants for the Southern Ocean, derived from surface experiments conducted during winter 2017. All the experiments were well-described by the Michaelis-Menten equation, provided that a location parameter, C, was included in the model. $V_{max}$ ranged from 5.2 ± 0.1 to 13 ± 0.4 nM $d^{-1}$ and $K_m$ ranged from 134 ± 8 to 403 ± 24 nM, with the latter parameter showing a strong positive relationship with the ambient $NO_2^-$ concentration. We interpret the positive values of C (range of 115 ± 2.3 to 245 ± 18 nM) to indicate an ambient $NO_2^-$ concentration threshold below which NOB, and thus $NO_2^-$ oxidation, are impeded. We hypothesize that this threshold indicates substrate limitation of NXR, possibly exacerbated by the low ambient iron concentrations characteristic of the upper Southern Ocean. Our kinetics experiments were conducted in surface waters only, which raises the question of the relevance of our findings for deeper euphotic zone waters. For instance, it is possible that surface nitrifier communities may be more iron limited than those living nearer the base of the euphotic zone. However, in the winter Southern Ocean, the euphotic zone is always considerably shallower than the mixed layer (50-75 m versus 100-250 m) such that both layers are typically very well-mixed, as is apparent from the near-invariant mixed-layer (and thus euphotic-

zone) distributions of nutrients (Fig 1b-c), including trace metals (Cloete et al., 2019). One might therefore expect the nitrifiers to also be evenly distributed over the euphotic zone and mixed layer. The light flux will not be homogenous over these layers, however. Indeed, light availability is frequently invoked to explain the vertical distribution of nitrification rates because nitrifier activity is impeded at high light (Horrigan et al., 1981; Olson, 1981b; Qin et al., 2014; Peng et al., 2018). Our nitrification depth profiles do not show a vertical trend, instead remaining similar throughout the euphotic zone and only rising near the base of the mixed layer (Figure 3b-e). We thus consider the results of our surface kinetics experiments to be broadly applicable to the euphotic zone in winter. From the depth-profile measurements, we deduce that the rate-limiting step for mixed-layer nitrification in the winter Southern Ocean is $NO_2^-$ oxidation. Despite this, $NO_3^-$ production from $NO_2^-$ oxidation accounted for 63-237% of the $NO_3^-$ consumed by phytoplankton, consistent with previous wintertime observations from the Atlantic sector (Mdutyana et al., 2020). The implication of this finding is that most of the mixed-layer $NO_3^-$ consumed by phytoplankton in winter, and likely also a significant fraction assimilated in spring, supports regenerated rather than new production (Yool et al., 2007; Mdutyana et al., 2020).

$NO_2^-$ oxidation, as the ultimate pathway connecting reduced N to its most oxidized form ($NO_3^-$), is important throughout the water column, but particularly in the upper layer where the supply of reduced N is highest. The production of $NO_3^-$ within the mixed layer from *in situ* nitrification can complicate the application of the new production paradigm as a framework for estimating carbon export potential, which advocates for additional measurements of this pathway over the upper ~200 m. Additionally, it is becoming increasingly clear that we lack a mechanistic understanding of the controls on nitrification (both $NH_4^+$ and $NO_2^-$ oxidation), which renders it challenging to model both its magnitude and distribution, as well as to assess how these may change in future. In particular, further study of the role of iron in controlling nitrification is required, particularly in the Southern Ocean where the mixed layer's biological N cycle is dominated by nitrification in winter (Smart et al., 2015; Mdutyana et al., 2020) and surface-layer iron remains scarce throughout the year (Tagliabue et al., 2012).

**Acknowledgements**

We thank Captain Knowledge Bengu and the crew of the R/V *S.A. Agulhas II* and Chief Scientist M. Vichi for professional support during the cruise, as well as the Marine Biogeochemistry Lab team at the University of Cape Town (UCT), C. Karriem for extensive administrative support, and I. Newton and J. Luyt at the UCT Stable Light Isotope Laboratory for filter analyses. The nitrification measurements were made possible through the Princeton University Visiting Student Research Collaborator program- we are especially grateful to S. Oleynik in the Department of Geosciences for his expert assistance during the first author's visit. This work was supported by the South African National Research Foundation through Antarctic Programme grants to S.E.F. (110735, 129232), and S.J.T. (93076), and postgraduate scholarships to M.M. (112380), T.M. (114673 and 130826) and J.M.B. (110732); by UCT

through a Harry Crossley Foundation Research Fellowship to M.M., postgraduate scholarship to T.M., Vice-Chancellor (VC) Research Scholarships to J.M.B., a VC Future Leaders 2030 award to S.E.F., and a Research Committee Equipment grant to S.E.F.; by the African Academy of Sciences/Royal Society through a FLAIR Fellowship to S.E.F; and by US National Science Foundation grants to B.B.W. The authors also acknowledge the South African Department of Science and Innovation's Biogeochemistry Research Infrastructure Platform.

## References


Amin, Shady A., James W. Moffett, Willm Martens-Habbena, Jeremy E. Jacquot, Yang Han, Allan Devol, Anitra E. Ingalls, David A. Stahl, and E. Virginia Armbrust. 2013. "Copper Requirements of the Ammonia-Oxidizing Archaeon Nitrosopumilus Maritimus SCM1 and Implications for Nitrification in the Marine Environment." *Limnology and Oceanography* 58 (6): 2037–45. https://doi.org/10.4319/lo.2013.58.6.2037.

Archontoulis, Sotirios V., and Fernando E. Miguez. 2014. "Nonlinear Regression Models and Applications in Agricultural Research." *Agronomy Journal* 107 (2): 786–98. https://doi.org/10.2134/agronj2012.0506.

Arp, Daniel J., Luis A. Sayavedra-Soto, and Norman G. Hommes. 2002. "Molecular Biology and Biochemistry of Ammonia Oxidation by Nitrosomonas Europaea." *Archives of Microbiology* 178 (4): 250–55. https://doi.org/10.1007/s00203-002-0452-0.

Baer, S. E., T. L. Connelly, R. E. Sipler, P. L. Yager, and D. A. Bronk. 2014. "Effect of Temperature on Rates of Ammonium Uptake and Nitrification in the Western Coastal Arctic during Winter, Spring, and Summer." *Global Biogeochemical Cycles* 28: 1455–66. https://doi.org/10.1111/1462-2920.13280.

Bayer, Barbara, Mak A. Saito, Matthew R. McIlvin, Sebastian Lücker, Dawn M. Moran, Thomas S. Lankiewicz, Christopher L. Dupont, and Alyson E. Santoro. 2021. "Metabolic Versatility of the Nitrite-Oxidizing Bacterium Nitrospira Marina and Its Proteomic Response to Oxygen-Limited Conditions." *ISME Journal* 15 (4): 1025–39. https://doi.org/10.1038/s41396-020-00828-3.

Belkin, Igor M., and Arnold L. Gordon. 1996. "Southern Ocean Fronts from the Greenwich Meridian to Tasmania." *Journal of Geophysical Research C: Oceans*. https://doi.org/10.1029/95JC02750.

Beman, J. Michael, Joy Leilei Shih, and Brian N. Popp. 2013. "Nitrite Oxidation in the Upper Water Column and Oxygen Minimum Zone of the Eastern Tropical North Pacific Ocean." *ISME Journal* 7 (11): 2192–2205. https://doi.org/10.1038/ismej.2013.96.

Beman, J. Michael, Brian N. Popp, and Christopher A. Francis. 2008. "Molecular and Biogeochemical Evidence for Ammonia Oxidation by Marine Crenarchaeota in the Gulf of California." *ISME Journal* 2 (4): 429–41. https://doi.org/10.1038/ismej.2007.118.

Bianchi, Micheline, F. Feliatra, Paul Tréguer, Marie Anne Vincendeau, and Jean Morvan. 1997. "Nitrification Rates, Ammonium and Nitrate Distribution in Upper Layers of the Water Column and in Sediments of the Indian Sector of the Southern Ocean." *Deep-Sea Research Part II: Topical Studies in Oceanography* 44 (5): 1017–32. https://doi.org/10.1016/S0967-0645(96)00109-9.

Birch, Colin P.D. 1999. "A New Generalized Logistic Sigmoid Growth Equation Compared with the Richards Growth Equation." *Annals of Botany* 83 (6): 713–23. https://doi.org/10.1006/anbo.1999.0877.

Blackburne, Richard, Vel M Vadivelu, and Zhiguo Yuan. 2007. "Kinetic Characterisation of an Enriched Nitrospira Culture with Comparison to Nitrobacter" 41: 3033–42. https://doi.org/10.1016/j.watres.2007.01.043.

Bock, Eberhard. 1965. "Vergleichende Untersuchungen Über Die Wirkung Sichtbaren Lichtes Auf Nitrosomonas Europaea Und Nitrobacter Winogradskyi." *Archiv Für Mikrobiologie*. https://doi.org/10.1007/BF00406848.

Bristow, Laura A., Tage Dalsgaard, Laura Tiano, Daniel B. Mills, Anthony D. Bertagnolli, Jody J. Wright, Steven J. Hallam, et al. 2016. "Ammonium and Nitrite Oxidation at Nanomolar Oxygen Concentrations in Oxygen Minimum Zone Waters." *Proceedings of the National Academy of Sciences* 113 (38): 10601–6. https://doi.org/10.1073/pnas.1600359113.

787 Bristow, Laura A., Neha Sarode, John Cartee, Alejandro Caro-Quintero, Bo Thamdrup, and Frank J.
788 Stewart. 2015. “Biogeochemical and Metagenomic Analysis of Nitrite Accumulation in the Gulf
789 of Mexico Hypoxic Zone.” *Limnology and Oceanography* 60 (5): 1733–50.
790 https://doi.org/10.1002/lno.10130.

791 Caranto, Jonathan D., and Kyle M. Lancaster. 2017. “Nitric Oxide Is an Obligate Bacterial
792 Nitrification Intermediate Produced by Hydroxylamine Oxidoreductase.” *Proceedings of the*
793 *National Academy of Sciences of the United States of America* 114 (31): 8217–22.
794 https://doi.org/10.1073/pnas.1704504114.

795 Carini, Paul, Christopher L. Dupont, and Alyson E. Santoro. 2018. “Patterns of Thaumarchaeal Gene
796 Expression in Culture and Diverse Marine Environments.” *Environmental Microbiology* 20 (6):
797 2112–24. https://doi.org/10.1111/1462-2920.14107.

798 Carvalho, Filipa, Josh Kohut, Matthew J. Oliver, and Oscar Schofield. 2017. “Defining the
799 Ecologically Relevant Mixed-Layer Depth for Antarctica’s Coastal Seas.” *Geophysical*
800 *Research Letters*. https://doi.org/10.1002/2016GL071205.

801 Cavagna, A. J., F. Fripiat, M. Elskens, P. Mangion, L. Chirurgien, I. Closset, M. Lasbleiz, et al. 2015.
802 “Production Regime and Associated N Cycling in the Vicinity of Kerguelen Island, Southern
803 Ocean.” *Biogeosciences* 12 (21): 6515–28. https://doi.org/10.5194/bg-12-6515-2015.

804 Clark, Darren R, Andrew P Rees, Ian Joint, Source Limnology, No Jan, Darren R Clark, Andrew P
805 Rees, and Ian Joint. 2008. “Ammonium Regeneration and Nitrification Rates in the Oligo
806 Trophic Atlantic Ocean : Implications for New Production Estimates.” *Limnology and*
807 *Oceanography* 53 (1): 52–62.

808 Cloete, R., J. C. Loock, T. Mtshali, S. Fietz, and A. N. Roychoudhury. 2019. “Winter and Summer
809 Distributions of Copper, Zinc and Nickel along the International GEOTRACES Section
810 GIPY05: Insights into Deep Winter Mixing.” *Chemical Geology* 511 (February 2018): 342–57.
811 https://doi.org/10.1016/j.chemgeo.2018.10.023.

812 Collos, Yves. 1998. “Nitrate Uptake, Nitrite Release and Uptake, and New Production Estimates.”
813 *Marine Ecology Progress Series* 171: 293–301. https://doi.org/10.3354/meps171293.

814 Damashek, Julian, Bradley B. Tolar, Qian Liu, Aimee O. Okotie-Oyekan, Natalie J. Wallsgrove,
815 Brian N. Popp, and James T. Hollibaugh. 2019. “Microbial Oxidation of Nitrogen Supplied as
816 Selected Organic Nitrogen Compounds in the South Atlantic Bight.” *Limnology and*
817 *Oceanography* 64 (3): 982–95. https://doi.org/10.1002/lno.11089.

818 DeVries, Tim, Mark Holzer, and Francois Primeau. 2017. “Recent Increase in Oceanic Carbon
819 Uptake Driven by Weaker Upper-Ocean Overturning.” *Nature* 542 (7640): 215–18.
820 https://doi.org/10.1038/nature21068.

821 Diaz, Frédéric, and Patrick Raimbault. 2000. “Nitrogen Regeneration and Dissolved Organic Nitrogen
822 Release during Spring in a NW Mediterranean Coastal Zone (Gulf of Lions): Implications for
823 the Estimation of New Production.” *Marine Ecology Progress Series* 197: 51–65.
824 https://doi.org/10.3354/meps197051.

825 DiFiore, Peter J., Daniel M. Sigman, and Robert B. Dunbar. 2009. “Upper Ocean Nitrogen Fluxes in
826 the Polar Antarctic Zone: Constraints from the Nitrogen and Oxygen Isotopes of Nitrate.”
827 *Geochemistry, Geophysics, Geosystems* 10 (11). https://doi.org/10.1029/2009GC002468.

828 Dore, John E, and David A I Karl. 1996. “Nitrification in the Euphotic Zone as a Source for Nitrite ,
829 Nitrate , and Nitrous Oxide at Station ALOHA” 41: 1619–28.

830 Dugdale, R. C., and J. J. Goering. 1967. “Uptake of New and Regenerated Forms of Nitrogen in
831 Primary Productivity.” *Limnology and Oceanography* 12 (2): 196–206.
832 https://doi.org/10.4319/lo.1967.12.2.0196.

Dugdale, R C, and F P Wilkerson. 1986. “The Use of N-15 To Measure Nitrogen Uptake in Eutrophic Oceans - Experimental Considerations.” *Limnology and Oceanography* 31 (4): 673–89.

Eppley, Richard W., and Bruce J. Peterson. 1979. “Particulate Organic Matter Flux and Planktonic New Production in the Deep Ocean.” *Nature* 282 (5740): 677–80. https://doi.org/10.1038/282677a0.

Fripiat, François, Anja S. Studer, Gerald H. Haug, Sergey Oleynik, Alfredo Martínez-García, Sandi M. Smart, Florian Rubach, Daniel M. Sigman, Sarah E. Fawcett, and Preston C. Kemeny. 2019. “The Isotope Effect of Nitrate Assimilation in the Antarctic Zone: Improved Estimates and Paleoceanographic Implications.” *Geochimica et Cosmochimica Acta* 247: 261–79. https://doi.org/10.1016/j.gca.2018.12.003.

Füssel, Jessika, Phyllis Lam, Gaute Lavik, Marlene M. Jensen, Moritz Holtappels, Marcel Günter, and Marcel M.M. Kuypers. 2012. “Nitrite Oxidation in the Namibian Oxygen Minimum Zone.” *ISME Journal* 6 (6): 1200–1209. https://doi.org/10.1038/ismej.2011.178.

Glibert, Patricia M., Mark R. Dennett, and Joel C. Goldman. 1985. “Inorganic Carbon Uptake by Phytoplankton in Vineyard Sound, Massachusetts. II. Comparative Primary Productivity and Nutritional Status of Winter and Summer Assemblages.” *Journal of Experimental Marine Biology and Ecology* 86 (2). https://doi.org/10.1016/0022-0981(85)90025-5.

Glibert, Patricia M., Fredric Lipschultz, James J. Mccarthy, and Mark A. Altabet. 1982. “Isotope Dilution Models of Uptake and Remineralization of Ammonium By Marine Plankton.” *Limnology and Oceanography* 27 (4): 639–50. https://doi.org/10.4319/lo.1982.27.4.0639.

Grasshoff K, Ehrhardt M, and, Kremling K. 1983. *Methods of Seawater Analysis*. Verlag Chemie, New York.

Gruber, Nicolas, Dominic Clement, Brendan R. Carter, Richard A. Feely, Steven van Heuven, Mario Hoppema, Masao Ishii, et al. 2019. “The Oceanic Sink for Anthropogenic CO 2 from 1994 to 2007.” *Science* 363 (6432): 1193–99. https://doi.org/10.1126/science.aau5153.

Haas, Sebastian, Brent M. Robicheau, Subhadeep Rakshit, Jennifer Tolman, Christopher K. Algar, Julie LaRoche, and Douglas W.R. Wallace. 2021. “Physical Mixing in Coastal Waters Controls and Decouples Nitrification via Biomass Dilution.” *Proceedings of the National Academy of Sciences of the United States of America* 118 (18). https://doi.org/10.1073/pnas.2004877118.

Hauck, J., C. Völker, D. A. Wolf-Gladrow, C. Laufkötter, M. Vogt, O. Aumont, L. Bopp, et al. 2015. “On the Southern Ocean CO2 Uptake and the Role of the Biological Carbon Pump in the 21st Century.” *Global Biogeochemical Cycles* 29 (9): 1451–70. https://doi.org/10.1002/2015GB005140.

Heiss, Elise M., and Robinson W. Fulweiler. 2017. “Erratum to ‘Coastal Water Column Ammonium and Nitrite Oxidation Are Decoupled in Summer’ (Estuarine, Coastal and Shelf Science (2016) 178 (110–119) (S0272771417301981) (10.1016/j.Ecss.2017.02.023)).” *Estuarine, Coastal and Shelf Science* 193: 37–45. https://doi.org/10.1016/j.ecss.2016.12.026.

Holmes, R M, A Aminot, R Kerouel, B A Hooker, and B J Peterson. 1999. “A Simple and Precise Method for Measuring Ammonium in Marine and Freshwater Ecosystems.” *Canadian Journal of Fisheries and Aquatic Sciences*. https://doi.org/10.1139/cjfas-56-10-1801.

Horak, Rachel E.A., Wei Qin, Andy J. Schauer, E. Virginia Armbrust, Anitra E. Ingalls, James W. Moffett, David A. Stahl, and Allan H. Devol. 2013. “Ammonia Oxidation Kinetics and Temperature Sensitivity of a Natural Marine Community Dominated by Archaea.” *ISME Journal* 7 (10): 2023–33. https://doi.org/10.1038/ismej.2013.75.

Horrigan, S. G., J. P. Montoya, J. L. Nevins, J. J. McCarthy, H. Ducklow, R. Goericke, and T. Malone. 1990. “Nitrogenous Nutrient Transformations in the Spring and Fall in the Chesapeake

879 Bay." *Estuarine, Coastal and Shelf Science* 30 (4). https://doi.org/10.1016/0272-7714(90)90004-
880 B.

881 Jacob, Juliane, Boris Nowka, Véronique Merten, Tina Sanders, Eva Spieck, and Kirstin Dähnke.
882 2017. "Oxidation Kinetics and Inverse Isotope Effect of Marine Nitrite-Oxidizing Isolates."
883 *Aquatic Microbial Ecology* 80 (3): 289–300. https://doi.org/10.3354/ame01859.

884 Jong, Ehlke de, Marcello Vichi, Carolin Birgitta Mehlmann, Clare Eayrs, Wade De Kock, Marcel
885 Moldenhauer, and Riesna Reuben Audh. 2018. "Sea Ice Conditions within the Antarctic
886 Marginal Ice Zone in Winter 2017, Onboard the SA Agulhas II." *Pangaea*, 2018.
887 https://doi.org/10.1594/PANGAEA.885211.

888 Kalvelage, Tim, Gaute Lavik, Phyllis Lam, Sergio Contreras, Lionel Arteaga, Carolin R. Löscher,
889 Andreas Oschlies, Aurélien Paulmier, Lothar Stramma, and Marcel M.M. Kuypers. 2013.
890 "Nitrogen Cycling Driven by Organic Matter Export in the South Pacific Oxygen Minimum
891 Zone." *Nature Geoscience* 6 (3): 228–34. https://doi.org/10.1038/ngeo1739.

892 Kendall, Carol. 1998. "USGS -- Isotope Tracers -- Resources: Isotope Tracers in Catchment
893 Hydrology -- Chapter 16." *Isotope Tracers in Catchment Hydrology Elsevier Science B.V.*

894 Khatiwala, S., F. Primeau, and T. Hall. 2009. "Reconstruction of the History of Anthropogenic CO2
895 Concentrations in the Ocean." *Nature* 462 (7271): 346–49. https://doi.org/10.1038/nature08526.

896 Kiefer, D. A., R. J. Olson, and O. Holm-Hansen. 1976. "Another Look at the Nitrite and Chlorophyll
897 Maxima in the Central North Pacific." *Deep-Sea Research and Oceanographic Abstracts* 23
898 (12). https://doi.org/10.1016/0011-7471(76)90895-0.

899 Kits, K. Dimitri, Christopher J. Sedlacek, Elena V. Lebedeva, Ping Han, Alexandr Bulaev, Petra
900 Pjevac, Anne Daebeler, et al. 2017. "Kinetic Analysis of a Complete Nitrifier Reveals an
901 Oligotrophic Lifestyle." *Nature* 549 (7671): 269–72. https://doi.org/10.1038/nature23679.

902 Kitzinger, Katharina, Hannah K. Marchant, Laura A. Bristow, Craig W. Herbold, Cory C. Padilla,
903 Abiel T. Kidane, Sten Littmann, et al. 2020. "Single Cell Analyses Reveal Contrasting Life
904 Strategies of the Two Main Nitrifiers in the Ocean." *Nature Communications* 11 (1).
905 https://doi.org/10.1038/s41467-020-14542-3.

906 Kowalchuk, G. A., and J. R. Stephen. 2001. "Ammonia-Oxidizing Bacteria: A Model for Molecular
907 Microbial Ecology." *Annual Review of Microbiology* 55: 485–529.
908 https://doi.org/10.1146/annurev.micro.55.1.485.

909 Kozlowski, Jessica A., Michaela Stieglmeier, Christa Schleper, Martin G. Klotz, and Lisa Y. Stein.
910 2016. "Pathways and Key Intermediates Required for Obligate Aerobic Ammonia-Dependent
911 Chemolithotrophy in Bacteria and Thaumarchaeota." *ISME Journal* 10 (8): 1836–45.
912 https://doi.org/10.1038/ismej.2016.2.

913 Lomas, Michael W., and Fredric Lipschultz. 2006. "Forming the Primary Nitrite Maximum: Nitrifiers
914 or Phytoplankton?" *Limnology and Oceanography* 51 (5): 2453–67.
915 https://doi.org/10.4319/lo.2006.51.5.2453.

916 Lücker, Sebastian, Michael Wagner, Frank Maixner, Eric Pelletier, Hanna Koch, Benoit Vacherie,
917 Thomas Rattei, et al. 2010. "A Nitrospira Metagenome Illuminates the Physiology and
918 Evolution of Globally Important Nitrite-Oxidizing Bacteria." *Proceedings of the National*
919 *Academy of Sciences of the United States of America* 107 (30): 13479–84.
920 https://doi.org/10.1073/pnas.1003860107.

921 Martens-Habbena, Willm, Paul M. Berube, Hidetoshi Urakawa, José R. De La Torre, and David A.
922 Stahl. 2009. "Ammonia Oxidation Kinetics Determine Niche Separation of Nitrifying Archaea
923 and Bacteria." *Nature* 461 (7266): 976–79. https://doi.org/10.1038/nature08465.

924 McIlvin, Matthew R., and Karen L. Casciotti. 2011. "Technical Updates to the Bacterial Method for

Nitrate Isotopic Analyses." *Analytical Chemistry* 83 (5): 1850–56. https://doi.org/10.1021/ac1028984.

Mdutyana, Mhlangabezi. 2021. "Mixed Layer Nitrogen Cycling in the Southern Ocean: Seasonality, Kinetics, and Biogeochemical Implications A Thesis Presented for the Degree Of." *University of Cape Town, PhD Thesis*, no. June.

Mdutyana, Mhlangabezi, Xin Sun, Jessica Burger, Raquel Flynn, Shantelle Smith, Natasha R. van Horsten, Eva Bucciarelli, et al. 2022. "The Kinetics of Ammonium Uptake and Oxidation during Winter across the Indian Sector of the Southern Ocean." *Limnology and Oceanography*, 1–19. https://doi.org/10.1002/lno.12050.

Mdutyana, Mhlangabezi, Sandy J. Thomalla, R. Philibert, Bess B. Ward, and Sarah E. Fawcett. 2020. "The Seasonal Cycle of Nitrogen Uptake and Nitrification in the Atlantic Sector of the Southern Ocean." *Global Biogeochemical Cycles*, no. 3: 1–29. https://doi.org/10.1029/2019GB006363.

Meincke, Michael, Eberhard Bock, Dieter Kastrau, and Peter M.H. Kroneck. 1992. "Nitrite Oxidoreductase from Nitrobacter Hamburgensis: Redox Centers and Their Catalytic Role." *Archives of Microbiology* 158 (2): 127–31. https://doi.org/10.1007/BF00245215.

Milligan, Allen J., and Paul J. Harrison. 2000. "Effects of Non-Steady-State Iron Limitation on Nitrogen Assimilatory Enzymes in the Marine Diatom Thalassiosira Weissflogii (Bacillariophyceae)." *Journal of Phycology* 36 (1): 78–86. https://doi.org/10.1046/j.1529-8817.2000.99013.x.

Monod, Jacques. 1942. "Recherches Sur La Croissance Des Cultures Bacteriennes." *Hermann and Cie, Paris.*

Mulholland, Margaret R., and Peter W. Bernhardt. 2005. "The Effect of Growth Rate, Phosphorus Concentration, and Temperature on N2 Fixation, Carbon Fixation, and Nitrogen Release in Continuous Cultures of Trichodesmium IMS101." *Limnology and Oceanography* 50 (3): 839–49. https://doi.org/10.4319/lo.2005.50.3.0839.

Newell, Silvia E., Andrew R. Babbin, Amal Jayakumar, and Bess B. Ward. 2011. "Ammonia Oxidation Rates and Nitrification in the Arabian Sea." *Global Biogeochemical Cycles* 25 (4): 1–10. https://doi.org/10.1029/2010GB003940.

Newell, Silvia E., Sarah E. Fawcett, and Bess B. Ward. 2013. "Depth Distribution of Ammonia Oxidation Rates and Ammonia-Oxidizer Community Composition in the Sargasso Sea." *Limnology and Oceanography* 58 (4): 1491–1500. https://doi.org/10.4319/lo.2013.58.4.1491.

Nowka, Boris, Holger Daims, and Eva Spieck. 2015. "Comparison of Oxidation Kinetics of Nitrite-Oxidizing Bacteria : Nitrite Availability as a Key Factor in Niche Differentiation" 81 (2): 745–53. https://doi.org/10.1128/AEM.02734-14.

Olsen, Are, Alex Kozyr, Siv K. Lauvset, Mario Hoppema, Fiz F. Pérez, Reiner Steinfeldt, Sara Jutterström, et al. 2016. "The Global Ocean Data Analysis Project Version 2 (GLODAPv2) – an Internally Consistent Data Product for the World Ocean." *Earth System Science Data* 8 (2): 297–323. https://doi.org/10.5194/essd-8-297-2016.

Olson, RJ. 1981a. "15N Tracer Studies of the Primary Nitrite Maximum." *Journal of Marine Research* 39 (Number 2): 203–26.

———. 1981b. "Differential Photoinhibition of Marine Nitrifying Bacteria - a Possible Mechanism for the Formation of the Primary Nitrite Maximum." *Journal of Marine Research* 39 (2): 227–38.

Orsi, H, Thomas Whitworth, and Worth D Nowlin Jr. 1995. "On the Meridional Extent and Fronts of the Antarctic Circumpolar Current Pronounced Meridional Gradients in Surface Properties Separate Waters of the Southern Ocean from the Warmer and Saltier Waters of the Subtropical

971 Circulations." *Deep Sea Research* 42 (5): 641–73. https://doi.org/10.1016/0967-0637(95)00021-
972 W.

973 Pachiadaki, Maria G, Eva Sintes, Kristin Bergauer, Julia M Brown, Nicholas R Record, Brandon K
974 Swan, and Mary Elizabeth Mathyer. 2017. "Major Role of Nitrite-Oxidizing Bacteria in Dark
975 Ocean Carbon Fixation" 1051 (November): 1046–51.

976 Pasciak, Walter J, and Jerome Gavis. 1974. "Transport Limitation of Nutrient Uptake in
977 Phytoplankton." *Limnology and Oceanography* 19 (6): 881–88.

978 Peng, Xuefeng, Sarah E. Fawcett, Nicolas van Oostende, Martin J. Wolf, Dario Marconi, Daniel M.
979 Sigman, and Bess B. Ward. 2018. "Nitrogen Uptake and Nitrification in the Subarctic North
980 Atlantic Ocean." *Limnology and Oceanography*, no. 1967. https://doi.org/10.1002/lno.10784.

981 Peng, Xuefeng, Clara A. Fuchsman, Amal Jayakumar, Sergey Oleynik, Willm Martens-Habbena,
982 Allan H. Devol, and Bess B. Ward. 2015. "Ammonia and Nitrite Oxidation in the Eastern
983 Tropical North Pacific." *Global Biogeochemical Cycles* 29 (12): 2034–49.
984 https://doi.org/10.1002/2015GB005278.

985 Peng, Xuefeng, Clara A. Fuchsman, Amal Jayakumar, Mark J. Warner, Allan H. Devol, and Bess B.
986 Ward. 2016. "Revisiting Nitrification in the Eastern Tropical South Pacific: A Focus on
987 Controls." *Journal of Geophysical Research: Oceans*. https://doi.org/10.1002/2015JC011455.

988 Philibert, R., H. Waldron, and D. Clark. 2015. "A Geographical and Seasonal Comparison of
989 Nitrogen Uptake by Phytoplankton in the Southern Ocean." *Ocean Science* 11 (2): 251–67.
990 https://doi.org/10.5194/os-11-251-2015.

991 Pollard, R. T., M. I. Lucas, and J. F. Read. 2002. "Physical Controls on Biogeochemical Zonation in
992 the Southern Ocean." *Deep-Sea Research Part II: Topical Studies in Oceanography* 49 (16):
993 3289–3305. https://doi.org/10.1016/S0967-0645(02)00084-X.

994 Qin, Wei, Shady A. Amin, Rachel A. Lundeen, Katherine R. Heal, Willm Martens-Habbena, Serdar
995 Turkarslan, Hidetoshi Urakawa, et al. 2018. "Stress Response of a Marine Ammonia-Oxidizing
996 Archaeon Informs Physiological Status of Environmental Populations." *ISME Journal* 12 (2):
997 508–19. https://doi.org/10.1038/ismej.2017.186.

998 Qin, Wei, Shady A. Amin, Willm Martens-Habbena, Christopher B. Walker, Hidetoshi Urakawa,
999 Allan H. Devol, Anitra E. Ingalls, James W. Moffett, E. Virginia Armbrust, and David A. Stahl.
1000 2014. "Marine Ammonia-Oxidizing Archaeal Isolates Display Obligate Mixotrophy and Wide
1001 Ecotypic Variation." *Proceedings of the National Academy of Sciences of the United States of*
1002 *America* 111 (34): 12504–9. https://doi.org/10.1073/pnas.1324115111.

1003 Raven, J. A., and P. G. Falkowski. 1999. "Oceanic Sinks for Atmospheric CO2." *Plant, Cell and*
1004 *Environment* 22 (6): 741–55. https://doi.org/10.1046/j.1365-3040.1999.00419.x.

1005 Read, J. F., R. T. Pollard, and U. Bathmann. 2002. "Physical and Biological Patchiness of an Upper
1006 Ocean Transect from South Africa to the Ice Edge near the Greenwich Meridian." *Deep-Sea*
1007 *Research Part II: Topical Studies in Oceanography* 49 (18): 3713–33.
1008 https://doi.org/10.1016/S0967-0645(02)00108-X.

1009 Rees, Andrew P., Ian Joint, and Kirsten M. Donald. 1999. "Early Spring Bloom Phytoplankton-
1010 Nutrient Dynamics at the Celtic Sea Shelf Edge." *Deep-Sea Research Part I: Oceanographic*
1011 *Research Papers*. https://doi.org/10.1016/S0967-0637(98)00073-9.

1012 Saito, Mak A., Matthew R. McIlvin, Dawn M. Moran, Alyson E. Santoro, Chris L. Dupont, Patrick A.
1013 Rafter, Jaclyn K. Saunders, et al. 2020. "Abundant Nitrite-Oxidizing Metalloenzymes in the
1014 Mesopelagic Zone of the Tropical Pacific Ocean." *Nature Geoscience* 13 (5): 355–62.
1015 https://doi.org/10.1038/s41561-020-0565-6.

1016 Santoro, A. E., C. M. Sakamoto, J. M. Smith, J. N. Plant, A. L. Gehman, A. Z. Worden, K. S.

Johnson, C. A. Francis, and K. L. Casciotti. 2013. “Measurements of Nitrite Production in and around the Primary Nitrite Maximum in the Central California Current.” *Biogeosciences* 10 (11): 7395–7410. https://doi.org/10.5194/bg-10-7395-2013.

Santoro, Alyson E., Christopher L. Dupont, R. Alex Richter, Matthew T. Craig, Paul Carini, Matthew R. McIlvin, Youngik Yang, William D. Orsi, Dawn M. Moran, and Mak A. Saito. 2015. “Genomic and Proteomic Characterization of ‘Candidatus Nitrosopelagicus Brevis’: An Ammonia-Oxidizing Archaeon from the Open Ocean.” *Proceedings of the National Academy of Sciences of the United States of America* 112 (4): 1173–78. https://doi.org/10.1073/pnas.1416223112.

Schaefer, Sylvia C., and James T. Hollibaugh. 2017. “Temperature Decouples Ammonium and Nitrite Oxidation in Coastal Waters.” *Environmental Science and Technology* 51 (6): 3157–64. https://doi.org/10.1021/acs.est.6b03483.

Schofield, Oscar, Travis Miles, Anne Carlijn Alderkamp, Sang Hoon Lee, Christina Haskins, Emily Rogalsky, Rachel Sipler, Robert M. Sherrell, and Patricia L. Yager. 2015. “In Situ Phytoplankton Distributions in the Amundsen Sea Polynya Measured by Autonomous Gliders.” *Elementa*. https://doi.org/10.12952/journal.elementa.000073.

Sciandra, A., and R. Amara. 1994. “Effects of Nitrogen Limitation on Growth and Nitrite Excretion Rates of the Dinoflagellate Prorocentrum Minimum.” *Marine Ecology Progress Series* 105 (3): 301. https://doi.org/10.3354/meps105301.

Shafiee, Roxana T., Joseph T. Snow, Qiong Zhang, and Rosalind E. M. Rickaby. 2019. “Iron Requirements and Uptake Strategies of the Globally Abundant Marine Ammonia-Oxidising Archaeon, Nitrosopumilus Maritimus SCM1.” *The ISME Journal*. https://doi.org/10.1038/s41396-019-0434-8.

Sigman, D. M., K. L. Casciotti, M. Andreani, C. Barford, M. Galanter, and J. K. Böhlke. 2001. “A Bacterial Method for the Nitrogen Isotopic Analysis of Nitrate in Seawater and Freshwater.” *Analytical Chemistry* 73 (17): 4145–53. https://doi.org/10.1021/ac010088e.

Smart, Sandi M, Sarah E Fawcett, Sandy J Thomalla, Mira a Weigand, Chris J C Reason, and Daniel M Sigman. 2015. “Global Biogeochemical Cycles,” 1–19. https://doi.org/10.1002/2014GB005013.Received.

Smith, Shantelle, Katye E. Altieri, Mhlangabezi Mdutyana, David R. Walker, Ruan G. Parrott, Sedick Gallie, Kurt A.M. Spence, Jessica M. Burger, and Sarah E. Fawcett. 2022. “Biogeochemical Controls on Ammonium Accumulation in the Surface Layer of the Southern Ocean.” *Biogeosciences* 19 (3): 715–41. https://doi.org/10.5194/bg-19-715-2022.

Sorokin, Dimitry Y., Sebastian Lücker, Dana Vejmelkova, Nadezhda A. Kostrikina, Robbert Kleerebezem, W. Irene C. Rijpstra, Jaap S. Sinninghe Damsté, et al. 2012. “Nitrification Expanded: Discovery, Physiology and Genomics of a Nitrite-Oxidizing Bacterium from the Phylum Chloroflexi.” *ISME Journal* 6 (12): 2245–56. https://doi.org/10.1038/ismej.2012.70.

Spieck, Eva, Silke Ehrich, and Jens Aamand. 1998. “Isolation and Immunocytochemical Location of the Nitrite-Oxidizing System in Nitrospira Moscoviensis.” *Arch Microbiol*, no. 169: 225–30.

Sun, Xin, Claudia Frey, Emilio Garcia-Robledo, Amal Jayakumar, and Bess B. Ward. 2021. “Microbial Niche Differentiation Explains Nitrite Oxidation in Marine Oxygen Minimum Zones.” *The ISME Journal*, 1–13. https://doi.org/10.1038/s41396-020-00852-3.

Sun, Xin, Qixing Ji, Amal Jayakumar, and Bess B. Ward. 2017. “Dependence of Nitrite Oxidation on Nitrite and Oxygen in Low-Oxygen Seawater.” *Geophysical Research Letters* 44 (15): 7883–91. https://doi.org/10.1002/2017GL074355.

Sundermeyer-Klinger, Hilke, Wolfgang Meyer, Beate Warninghoff, and Eberhard Bock. 1984.

"Membrane-Bound Nitrite Oxidoreductase of Nitrobacter: Evidence for a Nitrate Reductase System." *Archives of Microbiology* 140 (2–3). https://doi.org/10.1007/BF00454918.

Tagliabue, A., T. Mtshali, O. Aumont, A. R. Bowie, M. B. Klunder, A. N. Roychoudhury, and S. Swart. 2012. "A Global Compilation of Dissolved Iron Measurements: Focus on Distributions and Processes in the Southern Ocean." *Biogeosciences* 9 (6): 2333–49. https://doi.org/10.5194/bg-9-2333-2012.

Tsoularis, A, and J Wallace. 2002. "Analysis of Logistic Growth Models." *Mathematical Biosciences* 179: 21–55.

Ushiki, Norisuke, Masaru Jinno, Hirotsugu Fujitani, Toshikazu Suenaga, Akihiko Terada, and Satoshi Tsuneda. 2017. "Nitrite Oxidation Kinetics of Two Nitrospira Strains : The Quest for Competition and Ecological Niche Differentiation." *Journal of Bioscience and Bioengineering* 123 (5): 581–89. https://doi.org/10.1016/j.jbiosc.2016.12.016.

Vaccaro, Ralph F, and John H Ryther. 1960. "Marine Phytoplankton and the Distribution of Nitrite in the Sea*." *ICES Journal of Marine Science* 25 (3): 260–71. https://doi.org/10.1093/icesjms/25.3.260.

Vajrala, Neeraja, Willm Martens-Habbena, Luis A. Sayavedra-Soto, Andrew Schauer, Peter J. Bottomley, David A. Stahl, and Daniel J. Arp. 2013. "Hydroxylamine as an Intermediate in Ammonia Oxidation by Globally Abundant Marine Archaea." *Proceedings of the National Academy of Sciences of the United States of America* 110 (3): 1006–11. https://doi.org/10.1073/pnas.1214272110.

Volk, T., and M. I. Hoffert. 1985. "Ocean Carbon Pumps: Analysis of Relative Strengths and Efficiencies in Ocean-Driven Atmospheric CO2 Changes." *The Carbon Cycle and Atmospheric CO*.

Walker, C. B., J. R. De La Torre, M. G. Klotz, H. Urakawa, N. Pinel, D. J. Arp, C. Brochier-Armanet, et al. 2010. "Nitrosopumilus Maritimus Genome Reveals Unique Mechanisms for Nitrification and Autotrophy in Globally Distributed Marine Crenarchaea." *Proceedings of the National Academy of Sciences of the United States of America* 107 (19): 8818–23. https://doi.org/10.1073/pnas.0913533107.

Ward, B. B. 2005. "Temporal Variability in Nitrification Rates and Related Biogeochemical Factors in Monterey Bay, California, USA." *Marine Ecology Progress Series* 292: 97–109. https://doi.org/10.3354/meps292097.

———. 2008. "Chapter 5 - Nitrification in Marine Systems." In *Nitrogen in the Marine Environment (2nd Edition)*, 199–261. https://doi.org/http://dx.doi.org/10.1016/B978-0-12-372522-6.00005-0.

Ward, B. B., and K. A. Kilpatrick. 1991. "Nitrogen Transformations in the Oxic Layer of Permanent Anoxic Basins: The Black Sea and the Cariaco Trench." In *Black Sea Oceanography*. https://doi.org/10.1007/978-94-011-2608-3_7.

Ward, B. B., and O. C. Zafiriou. 1988. "Nitrification and Nitric Oxide in the Oxygen Minimum of the Eastern Tropical North Pacific." *Deep Sea Research Part A, Oceanographic Research Papers* 35 (7): 1127–42. https://doi.org/10.1016/0198-0149(88)90005-2.

Watson, Andrew J., Ute Schuster, Jamie D. Shutler, Thomas Holding, Ian G.C. Ashton, Peter Landschützer, David K. Woolf, and Lonneke Goddijn-Murphy. 2020. "Revised Estimates of Ocean-Atmosphere CO2 Flux Are Consistent with Ocean Carbon Inventory." *Nature Communications* 11 (1): 1–6. https://doi.org/10.1038/s41467-020-18203-3.

Watson, Stanley W., Eberhard Bock, Frederica W. Valois, John B. Waterbury, and Ursula Schlosser. 1986. "Nitrospira Marina Gen. Nov. Sp. Nov.: A Chemolithotrophic Nitrite-Oxidizing Bacterium." *Archives of Microbiology*. https://doi.org/10.1007/BF00454947.

Watson, Stanley W., and John B. Waterbury. 1971. “Characteristics of Two Marine Nitrite Oxidizing Bacteria,.” *Microscopy* 77 (2631): 203–30.

Weigand, M. Alexandra, Julien Foriel, Bruce Barnett, Sergey Oleynik, and Daniel M. Sigman. 2016. “Updates to Instrumentation and Protocols for Isotopic Analysis of Nitrate by the Denitrifier Method.” *Rapid Communications in Mass Spectrometry* 30 (12): 1365–83. https://doi.org/10.1002/rcm.7570.

Xu, Min Nina, Xiaolin Li, Dalin Shi, Yao Zhang, Minhan Dai, Tao Huang, Patricia M. Glibert, and Shuh Ji Kao. 2019. “Coupled Effect of Substrate and Light on Assimilation and Oxidation of Regenerated Nitrogen in the Euphotic Ocean.” *Limnology and Oceanography* 64 (3): 1270–83. https://doi.org/10.1002/lno.11114.

Yool, Andrew, Adrian P Martin, Camila Fernández, and Darren R Clark. 2007. “The Significance of Nitrification for Oceanic New Production.” *Nature* 447 (7147): 999–1002. https://doi.org/10.1038/nature05885.

Zakem, Emily J., Alia Al-Haj, Matthew J. Church, Gert L. Van Dijken, Stephanie Dutkiewicz, Sarah Q. Foster, Robinson W. Fulweiler, Matthew M. Mills, and Michael J. Follows. 2018. “Ecological Control of Nitrite in the Upper Ocean.” *Nature Communications* 9 (1). https://doi.org/10.1038/s41467-018-03553-w.

Zhang, Yao, Wei Qin, Lei Hou, Emily J. Zakem, Xianhui Wan, Zihao Zhao, Li Liu, et al. 2020. “Nitrifier Adaptation to Low Energy Flux Controls Inventory of Reduced Nitrogen in the Dark Ocean.” *Proceedings of the National Academy of Sciences of the United States of America* 117 (9): 4823–30. https://doi.org/10.1073/pnas.1912367117.

## Tables and figures

**Table 1**: Kinetic parameters ($V_{max}$, $K_m$, and C) associated with $NO_2^-$ oxidation experiments conducted across the western Indian sector of the Southern Ocean in winter 2017. Included here is the best fit and 95% confidence interval ("CI") for each kinetic parameter, derived using a non-linear, least-squares optimization method (Scipy lmfit package, Python 3.7.6).

**Table 1**

| Station name | Latitude | Longitude | $[NO_2^-]_{amb}$ (nM) | $V_{max}$ (nM $d^{-1}$) | 95%CI (nM $d^{-1}$) | $K_m$ (nM) | 95%CI (nM) | C (nM) | 95%CI (nM) |
|---|---|---|---|---|---|---|---|---|---|
| St 01 | 37°S | 19°E | 157 | 9.1 | 7.9 to 10 | 263 | 192 to 350 | 193 | 144 to 206 |
| St 02 | 42°S | 21°E | 108 | 5.2 | 4.8 to 5.5 | 134 | 109 to 163 | 115 | 105 to 119 |
| St 03 | 45°S | 22°E | 103 | 8.3 | 7.4 to 9.3 | 206 | 15 to 373 | 139 | -11 to 163 |
| St 04 | 50°S | 26°E | 162 | 13 | 11 to 15 | 288 | 104 to 538 | 172 | 68 to 204 |
| St 05 | 55°S | 28°E | 212 | 14 | 13 to 15 | 329 | 183 to 458 | 245 | 138 to 272 |
| St 06 | 62°S | 30°E | 226 | 8.2 | 7.8 to 8.6 | 403 | 320 to 499 | 163 | 129 to 187 |
| St 07 | 62°S | 30°E | 226 | 6.6 | 6.0 to 7.4 | 317 | 234 to 395 | 237 | 190 to 255 |

**Table 2**: A selection of previously derived $K_m$ and $V_{max}$ values from the open ocean, along with the concurrently-measured ambient concentrations of nitrite ($[NO_2^-]_{amb}$). The numbers in parenthesis are standard errors.

**Table 2**

| Region | $[NO_2^-]$ (nM) | Sampled depth (m) | $K_m$ (nM) | $V_{max}$ (nM $d^{-1}$) | Reference |
|---|---|---|---|---|---|
| Indian Southern Ocean: St 01: 37°S | 157 | 7 | 263 (16) | 9.1 (0.5) | This study |
| Indian Southern Ocean: St 02: 42°S | 108 | 7 | 134 (8) | 5.2 (0.1) | This study |
| Indian Southern Ocean: St 03: 45°S | 103 | 7 | 206 (30) | 8.3 (0.4) | This study |
| Indian Southern Ocean: St 04:51°S | 162 | 7 | 288 (52) | 13 (0.7) | This study |
| Indian Southern Ocean: St 05: 56°S | 212 | 7 | 329 (29) | 14 (0.4) | This study |
| Indian Southern Ocean: St 06: 62°S | 226 | 7 | 403 (24) | 8.2 (0.1) | This study |
| Indian Southern Ocean: St 07: 62°S | 226 | 7 | 317 (20) | 6.6 (0.3) | This study |
| Southern California Bight | 20 | 60 | 70 | nd | Olson 1981 |
| Eastern Tropical North Pacific | 100 | 53 | 281 (151) | 63 (14) | Sun et al. 2017 |
| Eastern Tropical North Pacific | 50 | 170 | 227 (55) | 56 (5.4) | Sun et al. 2017 |
| South China Sea | 51 | 110 | 195 (33) | 30 (1.6) | Zhang et al. 2020 |
| South China Sea | 71 | 95 | 175 (37) | 24 (1.5) | Zhang et al. 2020 |
| South China Sea | 31 | 150 | 49 (15) | 9.6 (0.6) | Zhang et al. 2020 |
| South China Sea | 185 | 75 | 506 (82) | 12 (0.8) | Zhang et al. 2020 |
| South China Sea | 34 | 200 | 27 (11) | 4.6 (0.3) | Zhang et al. 2020 |
| Subtropical South Atlantic | 14 | 150 | 74 (29) | 22 (0.7) | Fawcett et al. unpubl. |
| Subtropical South Atlantic | 152 | 150 | 167 (4.3) | 27 (0.2) | Fawcett et al. unpubl. |

*nd represents not determined*

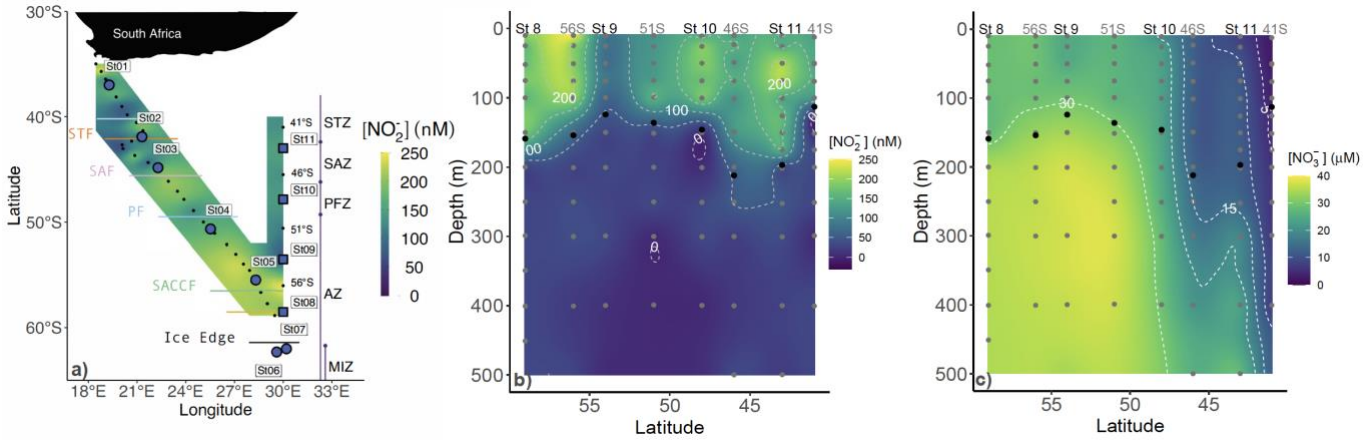


**Figure 1**: a) Map of the cruise track showing the kinetics stations (large circle symbols) and locations of the underway stations sampled during Leg 1 (small symbols), overlaid on the measured surface (~7 m) nitrite concentrations ($[NO_2^-]$). Additionally, the locations of the hydrocast stations occupied during Leg 2 are shown, with the stations at which depth-profile experiments were conducted shown by the large square symbols. The coloured horizontal lines denote the frontal positions at the time of sampling and the major zones of the Southern Ocean are indicated by the vertical lines and dots – STZ, Subtropical Zone; STF, Subtropical Front; SAZ, Subantarctic Zone; SAF, Subantarctic Front; PFZ, Polar Frontal Zone; PF, Polar Front; AZ, Antarctic Zone; SACCF, Southern Antarctic Circumpolar Front; MIZ, Marginal Ice Zone. Also shown are water column (0-500 m) profiles of the concentrations of b) nitrite ($NO_2^-$) and c) nitrate ($NO_3^-$) sampled during Leg 2. The grey dots indicate the discrete sampling depths at all the hydrocast stations (eight in total), with the four stations at which depth profile experiments were conducted (St 08 to St 11) labeled above the panel. The black dots show the derived mixed layer depths.

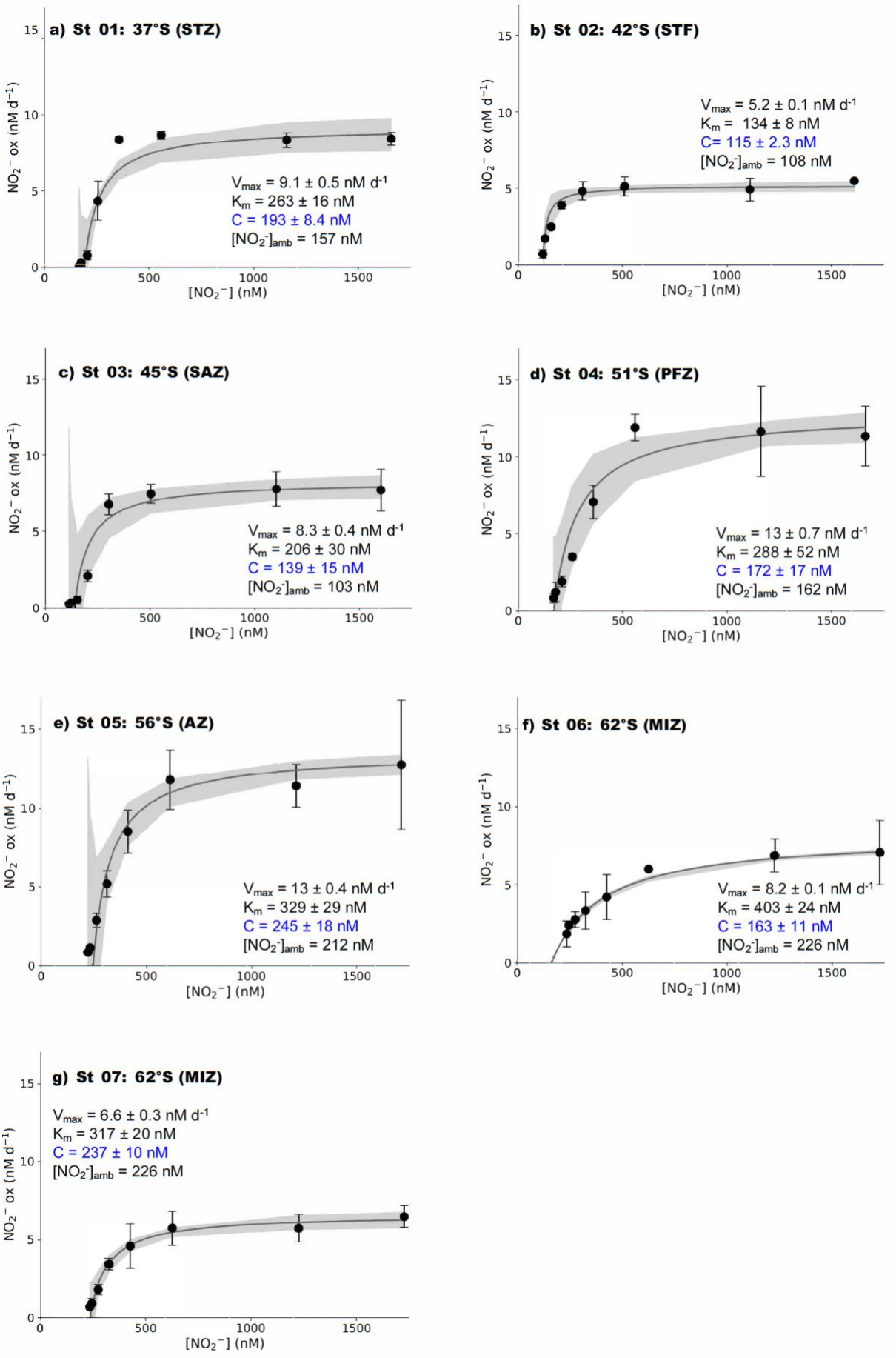
a) St 01: 37°S (STZ)
$V_{max}$ = 9.1 ± 0.5 nM d$^{-1}$
$K_m$ = 263 ± 16 nM
C = 193 ± 8.4 nM
[$NO_2^-$]$_{amb}$ = 157 nM
b) St 02: 42°S (STF)
$V_{max}$ = 5.2 ± 0.1 nM d$^{-1}$
$K_m$ = 134 ± 8 nM
C= 115 ± 2.3 nM
[$NO_2^-$]$_{amb}$ = 108 nM
c) St 03: 45°S (SAZ)
$V_{max}$ = 8.3 ± 0.4 nM d$^{-1}$
$K_m$ = 206 ± 30 nM
C = 139 ± 15 nM
[$NO_2^-$]$_{amb}$ = 103 nM
d) St 04: 51°S (PFZ)
$V_{max}$ = 13 ± 0.7 nM d$^{-1}$
$K_m$ = 288 ± 52 nM
C = 172 ± 17 nM
[$NO_2^-$]$_{amb}$ = 162 nM
e) St 05: 56°S (AZ)
$V_{max}$ = 13 ± 0.4 nM d$^{-1}$
$K_m$ = 329 ± 29 nM
C = 245 ± 18 nM
[$NO_2^-$]$_{amb}$ = 212 nM
f) St 06: 62°S (MIZ)
$V_{max}$ = 8.2 ± 0.1 nM d$^{-1}$
$K_m$ = 403 ± 24 nM
C = 163 ± 11 nM
[$NO_2^-$]$_{amb}$ = 226 nM
g) St 07: 62°S (MIZ)
$V_{max}$ = 6.6 ± 0.3 nM d$^{-1}$
$K_m$ = 317 ± 20 nM
C = 237 ± 10 nM
[$NO_2^-$]$_{amb}$ = 226 nM
$NO_2^-$ ox (nM d$^{-1}$)
[$NO_2^-$] (nM)

1173

**Figure 2:** Kinetics experiments: the dependence of the $NO_2^-$ oxidation rates on $NO_2^-$ concentration ($[NO_2^-]$) at the surface (~7 m) in winter at a) St 01: 37°S (STZ), b) St 02: 42°S (STF), c) St 03: 45°S (SAZ), d) St 04: 51°S (PFZ), e) St 05: 55°S (OAZ), f) St 06: 62°S (MIZ), and g) St 07: 62°S (MIZ). The solid lines show the Michaelis-Menten best fit, with the derived values of $V_{max}$, $K_m$, and C, as well as the ambient concentration of nitrite ($[NO_2^-]_{amb}$), indicated on each panel. Error bars represent the range of values, each measured at least twice. Where errors bars are not visible, they are smaller than the data markers. The grey shaded area shows the 95% confidence interval associated with the model fit. Note that the x-axis represents total $[NO_2^-]$ (i.e., $[^{15}NO_2^-]_{tracer}$ + $[NO_2^-]_{amb}$).

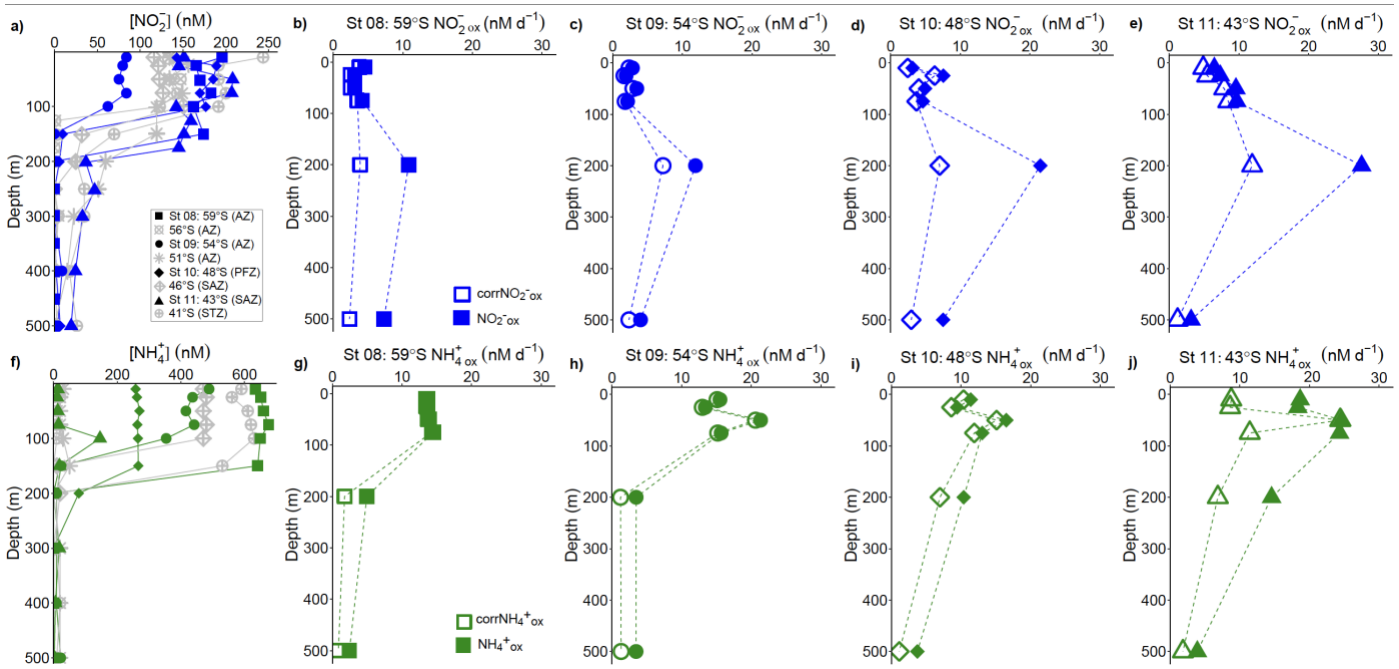


**Figure 3**: Depth-profile experiments: water column (0-500 m) profiles of the concentration of a) nitrite ($[NO_2^-]$) and f) ammonium ($[NH_4^+]$), and rates of $NO_2^-$ and $NH_4^+$ oxidation at b and g) St 08: 59°S (AZ), c and h) St 09: 54°S (AZ), d and i) St 10: 48°S (PFZ), and e and j) St 11: 43°S (SAZ). In panels a and f, the blue and green symbols indicate the stations at which oxidation rates were measured while the grey symbols show data from the stations where no experiments were conducted. In panels b-e and g-j, open symbols show the oxidation rates revised for possible stimulation due to $^{15}N$-tracer additions ($corrNO_2^-{}_{ox}$ and $corrNH_4^+{}_{ox}$; equation 4) and closed symbols show the uncorrected rates (equation 1). Error bars indicate the range of values, each measured at least twice. Where error bars are not visible, they are smaller than the data markers. The dashed lines connecting the data points are included only to guide the eye and should not be taken to imply interpolation with depth.

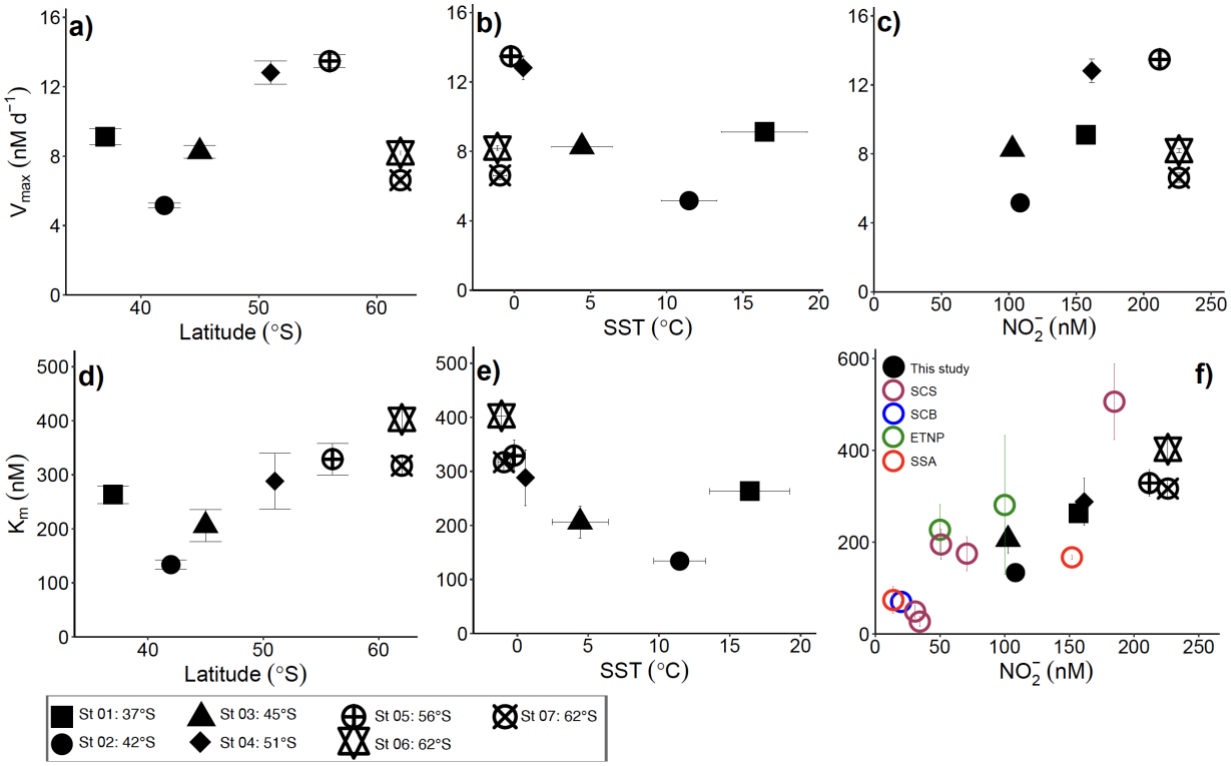


**Figure 4**: Potential controls on the kinetic parameters associated with $NO_2^-$ oxidation. $V_{max}$ and $K_m$ are shown as a function of a and d) latitude, b and e) sea surface temperature (SST), and c and f) the ambient nitrite concentration ($[NO_2^-]_{amb}$). Vertical error bars show the propagated error associated with $V_{max}$ and $K_m$ computed using a non-linear, least-squares optimization method (Scipy lmfit package, Python 3.7.6), while the symbols and horizontal error bars on panels b and e indicate the average (± 1 standard deviation) SST experienced by the sampled communities during the incubations. In panel f, black symbols show our Southern Ocean data, maroon symbols show $K_m$ values from the South China Sea (SCS; Zhang et al. 2020), the blue symbol shows the $K_m$ value derived for the South California Bight (SCB; Olson 1981a), the green symbol shows $K_m$ values from Eastern Tropical North Pacific oxygen deficient zone (ETNP; Sun et al. 2017), and the red symbols show $K_m$ values derived for the subtropical southeast Atlantic (SSA; Fawcett et al. unpubl.).

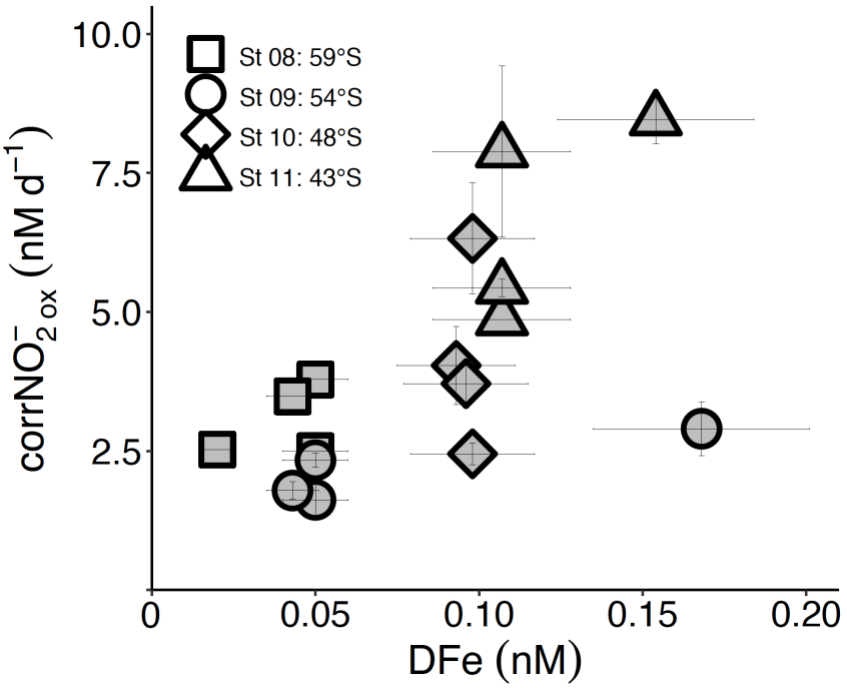


**Figure 5:** Euphotic zone (0-75 m) revised rates of $NO_2^-$ oxidation ($corrNO_{2\ ox}^-$) measured at the depth-profile stations (St 08 to St 11) plotted against coincident dissolved iron concentrations (DFe). Error bars indicate the range of values, each measured at least twice. Where errors bars are not visible, they are smaller than the data markers.

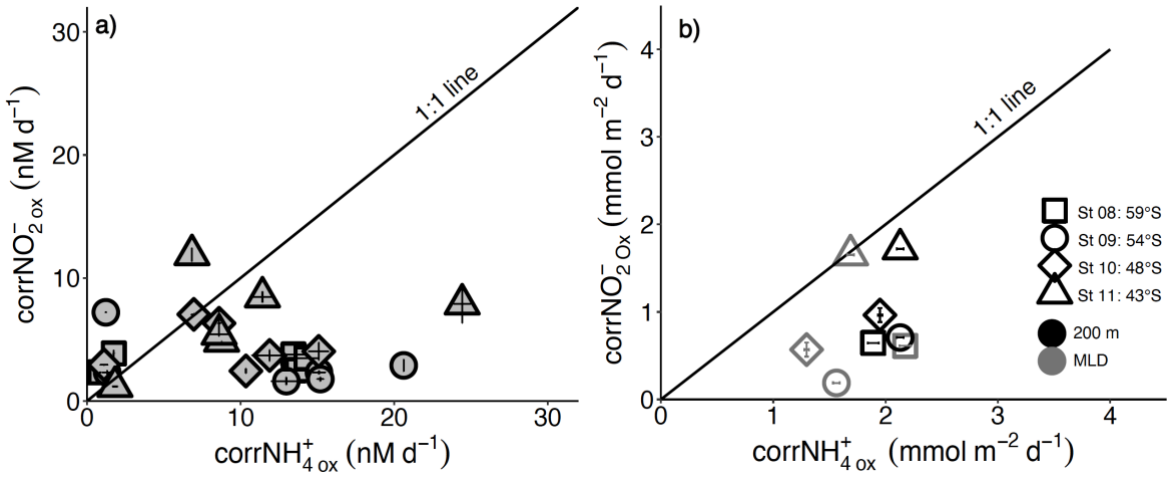


**Figure 6:** The relationship between the revised rates of $NO_2^-$ and $NH_4^+$ oxidation ($corrNO_{2\ ox}^-$ and $corrNH_{4\ ox}^+$) for a) each experiment depth in the upper water column (0-500 m) and b) integrated over the mixed layer (grey symbols) and upper 200 m (black symbols). Error bars on panel a indicate the range of values, each measured at least twice, while on panel b, error bars show the propagated error. Where errors bars are not visible, they are smaller than the data markers. The black diagonal line on both panels has a slope of 1, which is expected if the rates of $NH_4^+$ and $NO_2^-$ oxidation are tightly coupled.